AFFDL-TR-71-62
VOLUME IV
Part II

Volume IV. Wind Tunnel Test of the Conversion Process of a Folding Tilt-Rotor Aircraft Using a Semispan Unpowered Model

Part II. Blade Stress Analysis, Bench Tests, and Wind Tunnel Model Details

John Magee
Robert Taylor
The Boeing Company, Vertol Division
Philadelphia, Pennsylvania

TECHNICAL REPORT AFFDL-TR-71-62, VOLUME IV, PART II

August 1971

Air Force Flight Dynamics Laboratory
Air Force Systems Command
Wright-Patterson Air Force Base, Ohio

NOTICE

When Government drawings, specifications, or other data are used for any purpose other than in connection with a definitely related Government procurement operation, the United States Government thereby incurs no responsibility nor any obligation whatsoever; and the fact that the government may have formulated, furnished, or in any way supplied the said drawings, specifications, or other data, is not to be regarded by implication or otherwise as in any manner licensing the holder or any other person or corporation, or conveying any rights or permission to manufacture, use, or sell any patented invention that may in any way be related thereto.

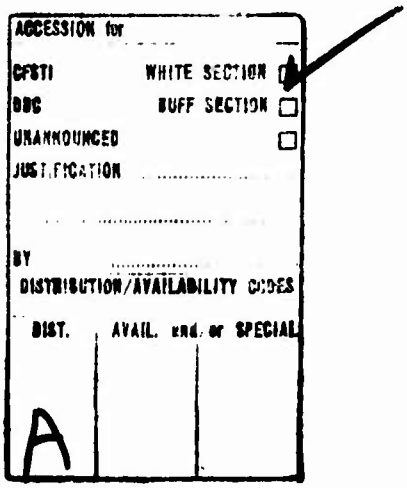

Copies of this report should not be returned unless return is required by security considerations, contractual obligations, or notice on a specific document.

14. KEY WORDS	LINK A		LINK B		LINK C	
	ROLE	WT	ROLE	WT	ROLE	WT
Folding tilt-rotor aircraft						
Blade stress analysis						
Bench tests						
Model description						
Wind tunnel test facility						

Unclassified
Security Classification

DOCUMENT CONTROL DATA - R & D

(Security classification of title, body of abstract and indexing annotation must be entered when the overall report is classified)

1. ORIGINATING ACTIVITY (Corporate author)	2a. REPORT SECURITY CLASSIFICATION
The Boeing Company, Vertol Division Boeing Center, P.O.Box 16858 Philadelphia, Pennsylvania 19142	Unclassified
	2b. GROUP -

3. REPORT TITLE

VOLUME IV. WIND TUNNEL TEST OF THE CONVERSION PROCESS OF A FOLDING TILT-ROTOR AIRCRAFT USING A SEMISPAN UNPOWERED MODEL - Part II. Blade Stress Analysis, Bench Tests, and Wind Tunnel Model Details

4. DESCRIPTIVE NOTES (Type of report and inclusive dates)

Final report

5. AUTHOR(S) (First name, middle initial, last name)

John Magee
Robert Taylor

6. REPORT DATE	7a. TOTAL NO. OF PAGES	7b. NO. OF REFS
August 1971	xiii + 74	None

8a. CONTRACT OR GRANT NO.	9a. ORIGINATOR'S REPORT NUMBER(S)
F33615-69-C-1577	D213-10000-4
b. PROJECT NO.	
c.	9b. OTHER REPORT NO(S) (Any other numbers that may be assigned this report)
d.	AFFDL-TR-71-62, Volume IV, Part II

10. DISTRIBUTION STATEMENT

Distribution of this document is unlimited.

11. SUPPLEMENTARY NOTES	12. SPONSORING MILITARY ACTIVITY
Volume IV of an 8-volume series	U.S. Air Force Flight Dynamics Lab Air Force Systems Command Wright-Patterson Air Force Base, Ohio

13. ABSTRACT

This document presents the detailed results of the blade stress analysis and the bench tests, as well as a description of the wind tunnel and the model. Mathematical findings are given in developed equations and in voluminous tabular data. Additional information is provided in the form of engineering graphs and curves, schematic diagrams, and photographs of the model and test setup. This volume is actually an appendix to Part I, Analysis and Results.

DD FORM 1 NOV 68 1473 REPLACES DD FORM 1473, 1 JAN 64, WHICH IS OBSOLETE FOR ARMY USE.

Unclassified
Security Classification

AFFDL-TR-71-62
Volume IV
Part II

VOLUME IV. WIND TUNNEL TEST OF THE CONVERSION PROCESS OF A FOLDING TILT-ROTOR AIRCRAFT USING A SEMISPAN UNPOWERED MODEL

Part II. Blade Stress Analysis, Bench Tests, and Wind Tunnel Model Details

John Magee

Robert Taylor

The Boeing Company, Vertol Division

Philadelphia, Pennsylvania

TECHNICAL REPORT AFFDL-TR-71-62, VOLUME IV, PART II

Air Force Flight Dynamics Laboratory

Air Force Systems Command

Wright-Patterson Air Force Base, Ohio

D213-10000-4

FOREWORD

This report was prepared by The Boeing Company, Vertol Division, Philadelphia, Pennsylvania, for the Air Force Flight Dynamics Laboratory, Wright-Patterson Air Force Base, Ohio, under Phase II of Contract F33615-69-C-1577. The contract was initiated under Project 69BT, "US/FRG Technology - V/STOL Aircraft Task 02," Prop/Rotor Technology. The contract objective is to develop design criteria and aerodynamic prediction techniques for the folding tilt-rotor concept through a program of model testing and analysis. This covers the first of four test programs which will be reported in separate volumes of the final report. Part II of this volume presents the blade stress analyses, model details, and bench tests. It was submitted by the authors in June 1971. The contract was administered by the Air Force Flight Dynamics Laboratory, Wright-Patterson Air Force Base, Ohio, with Mr. Daniel E. Fraga (AFFDL/FV) as Project Engineer.

The reports published under this contract for design studies and model tests of the Stowed Tilt Rotor concept are:

Volume I	Parametric Design Studies
Volume II	Component Design Studies
Volume III	Performance Data for Parametric Study Aircraft
Volume IV	Wind Tunnel Test of the Conversion Process of a Folding Tilt-Rotor Aircraft Using a Semispan Unpowered Model
Volume V	Wind Tunnel Test of a Powered Tilt Rotor Performance Model
Volume VI	Wind Tunnel Test of a Powered Tilt Rotor Dynamic Model on a Simulated Free Flight Suspension System
Volume VII	Wind Tunnel Test of the Dynamics and Aerodynamics of Rotor Spinup, Stopping and Folding on a Semispan Folding Tilt Rotor Model

Volume VIII Summary of Structural Design Criteria and Aerodynamic Prediction Techniques

The contractor's report number is D213-10000-4.

This technical report has been reviewed and is approved.

Ernest J. Cross Jr.

ERNEST J. CROSS, JR.
Lt. Colonel, USAF
Chief, V/STOL Technology Division

ABSTRACT

Wind tunnel test data obtained with a 33.75-inch diameter nonarticulated folding tilt rotor mounted on a semispan wing show the effects of collective pitch schedule variations on transient lift, drag, and pitching moment of the aircraft. Blade loads data presented show that loads do not limit the conversion process. The model was configured with prop/rotor blades which had an in-plane natural frequency of less than 1.0/rev. The testing included study of the aerodynamics and dynamics of rotor spin-up, spin-down, stopping, and steady windmilling. Correlation with predictions of transient aerodynamic performance, static derivatives of the prop/rotor, and blade loads are included. This part presents the detailed results of the blade stress analysis and the bench tests, as well as a description of the wind tunnel and the model. Mathematical findings are given in developed equations and in voluminous tabular data. Additional information is provided in the form of engineering graphs and curves, schematic diagrams, and photographs of the model and test setup. This volume is actually an appendix to Part I, Analysis and Results.

TABLE OF CONTENTS

LIST OF ILLUSTRATIONS

LIST OF TABLES

LIST OF SYMBOLS

b	Number of blades	—
c	Blade chord	ft
$\bar{c}$	Wing mean aerodynamic chord	ft
C_D	Drag coefficient $\frac{D}{qS}$	—
C_L	Lift coefficient $\frac{L}{qS}$	—
C_M	Pitching moment coefficient $\frac{M}{qS\bar{c}}$	—
D	Aerodynamic drag parallel to wind axis	lb
E	Modulus of elasticity (Young's Modulus)	lb/in^2
f_t	Tensile stress	lb/in^2
f_b	Bending stress	lb/in^2
GJ	Blade torsional stiffness	$lb\text{-}in^2$
I	Moment of inertia	$lb\text{-}ft\text{-}sec^2$
J	Propeller advance ratio, $\pi V/\Omega R$	—
k_θ	Spring rate	in-lb
L	Aerodynamic lift	lb
M	Aerodynamic pitching moment	ft-lb
M_c	Chord bending moment	in-lb

M_f	Flap bending moment	in-lb
q	Freestream dynamic pressure, $1/2\rho V^2$	lb/ft^2
r	Radius to a blade station	ft
R	Blade radius	ft
S	Wing reference area	ft^2
t	Blade section thickness	ft
V	Tunnel speed	ft/sec
W	Running blade weight	lb/in
x	Distance from blade centroid to vertical station	in
α	Wing and/or rotor angle of attack	degrees
δ	Wing flap deflection angle	degrees
ρ	Air density	$slugs/ft^3$
σ	Rotor solidity, $\frac{bc}{\pi R}$	—
θ_{75}	Blade collective pitch at .75R	degrees
θ_T	Blade twist caused by load application	degrees
Ω	Rotor angular velocity	rad/sec
ω_L	First mode, in-plane blade natural frequency	rad/sec

ω_β	First mode, flapwise blade natural frequency	rad/sec
$\Delta\theta$	Torsional deflection	degrees
Δf	Flapwise displacement	in
Δc	Chordwise deflection	in

SECTION I

INTRODUCTION

This report was prepared by The Boeing Company, Vertol Division, Philadelphia, Pennsylvania, for the Air Force Flight Dynamics Laboratory, Wright-Patterson Air Force Base, Ohio, under Phase II of Contract F33615-69-C-1577. The contract objective is to develop design criteria and aerodynamic prediction techniques for the folding tilt-rotor concept through a program of model testing and analysis. Part I of this report presents the analysis and results of the first of four test programs. Presented in this volume are the blade stress analysis, bench test results, and the model details. The blade stress analysis model design and fabrication were performed by Mr. W. Putman of the Forrestal Laboratories, Princeton University.

SECTION II

BLADE STRESS ANALYSIS

Presented in this section are the analyses of blade weights, inertia properties, and stresses. The analysis is performed for various radial stations as shown in Table I. The centrifugal force and torsion moment acting at each section are given in Table II; the appropriate geometry and properties are also presented in Tables III through V. The material stresses were found to be less than the allowable stress based on 10-hour life. A preliminary analysis showed that the root sections were not structurally adequate as built and required additional strengthening with an aluminum and fiberglass band as shown in Figures 1 and 2.

TABLE I

STIFFNESS AND STRESS SUMMARY (ROOT FITTING AND TIP)

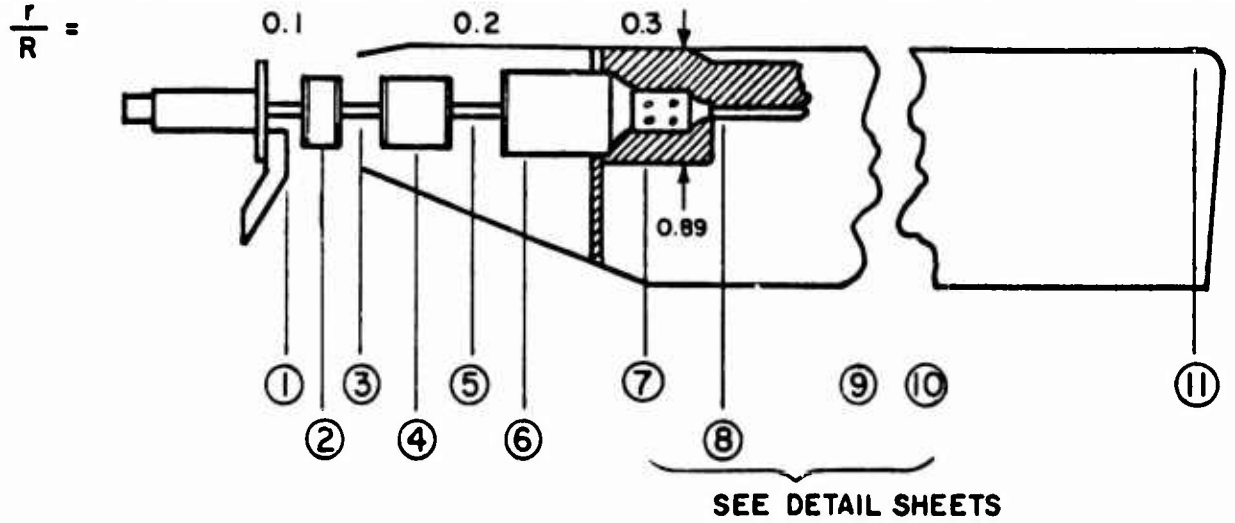

SEE DETAIL SHEETS

Section	r/R	Shape and Materials	EI, lb-in²		GJ lb-in²	Area in²	Stresses, Kps:				
							Steady Stress		Alternating Stress		
			Flap	Chord			Tensile	Shear	Flap	Chord	Tota
①	.091 to .113	4130 STEEL; 1.00; 0.048	128 x10³	270	48x10³	.048	3.54	0.32	1.6	20.2	21.8
②	.116 to .142	0.080; 4130 STEEL; 0.625	780	45 x10³	17x10³	.050	3.30	0.55	20.4	1.5	21.9
③	.145 to .160	4130 STEEL; 0.50; 0.084	21 x10³	720	7.9x10	.042	3.81	0.91	4.6	12.5	17.1
④	.163 to .195	0.077; 4130 STEEL; 0.625	690	43 x10³	16x10³	.048	3.12	0.54	19.6	1.5	21.1
⑤	.198 to .225	4130 STEEL; 0.361; 0.250; 0.120	13 to 4.4 x10³	1370 to 1040	4.9x10³ to 1.7x10³	.043 to .030	3.26 to 4.66	0.90 to 1.65	2.9 to 9.6	8.8 to 11.5	11.7 to 21.1
⑥	.228 to .287	0.075; 4130 STEEL; 0.625	640	41 x10³	15x10³	.047	2.76	0.52	18.5	1.4	19.9
⑪	0.98	0.16	281	32 x10³	242	.022 to .012	0.29	0	0.4	0	0.4

TABLE II

DESIGN LOADS

Section	$\frac{r}{R}$	Centrifugal Force, lb.	Torsion, in - lb	Flapping Moment, in - lb	Chordwise Moment, in - lb
①	.10	170	2.80	14.4	7.8
②	.12	165	2.75	13.8	7.6
③	.14	160	2.70	13.2	7.4
④	.17	150	2.60	12.4	7.2
⑤	.20	140	2.50	11.5	6.9
⑥	.23	130	2.40	11.0	6.6
⑦	.30	110	2.20	10.0	6.0
⑧	.34	100	2.10	9.5	5.7
⑨	.43	87	1.80	8.2	4.9
⑩	.55	70	1.40	6.5	3.9
⑪	.98	10	0.10	0.4	0.2

TABLE III

BLADE GEOMETRY

Section	I_{flap}	I_{chord}	c_{flap}	c_{chord}	$\frac{c}{I_{flap}}$	$\frac{c}{I_{chord}}$	J	$\frac{c_{max}}{J}$
	$x10^6$, in^4		in		$1/in^3 \times 10^{-3}$		$x10^3$	$x10^{-3}$
①	4400	9.3	.500	.024	.11	2.58	4.40	.113
②	27	1550	.040	.312	1.48	.20	1.55	.201
③	724	25	.250	.042	.35	1.68	.75	.333
④	24	1480	.038	.312	1.58	.21	1.50	.208
⑤	448 to 151	47 to 36	.180 to .125	.060	.25 to .83	1.28 to 1.67	.50 to .19	.360 to .660
⑥	22	1410	.037	.312	1.68	.22	1.43	.218

TABLE IV
BLADE PROPERTIES

ρ_{STEEL} = .283 lb/in^3 , ρ_{Al} = .101 lb/in^3 , ρ_{GLASS} = .05[illegible] $_{WFP}$ lb/in^3,

E_{STEEL} = 29 X 10^6 , G_{STEEL} = 11.0 X 10^6

Section	r/R	A_1 in^2	W_1 lb/in	θ_{WPT} .75r
①	.091 - .113	0.0[illegible]3	.013[illegible]	- 10°
① ②	.113 - .11[illegible]	0.[illegible]	.1[illegible]	- 10°
②	.11[illegible] - .142	0.0[illegible]0	.01[illegible]	- 10°
② ③	.142 - .145	0.[illegible]00	.0[illegible]	- 10°
③	.145 - .1[illegible]0	0.0[illegible]	.011[illegible]	- 10°
③ ④	.1[illegible]0 - .1[illegible]3	0.[illegible]00	.0[illegible]	- 10°
④	.1[illegible]3 - .195	0.0[illegible]3	.013[illegible]	- 10°
④ ⑤	.195 - .19[illegible]	0.2[illegible]3	.0[illegible]3	+ 1[illegible].8°
⑤	.19[illegible] - .225	.043 - 0.30[illegible]	.01[illegible]-.00[illegible]	14.8°
⑤ ⑥	.225 - .228	0.14[illegible]	.0[illegible]2	14.8°
⑥	.228 - .28[illegible]	0.0[illegible]	.0133	14.8°
⑦	.2[illegible] - .330	FOAM & FINISH 0.0024 0.016 STEEL 0.0045 0.019 AL. 0.0019 } 0.114 0.045 GLASS 0.0026		14.8°
⑧	.340	0.067 GLASS 0.0039 0.003 STEEL 0.0008 } 0.0071 F&F 0.0024		14.1°
⑨	.430	0.036 GLASS 0.0021 } 0.0053 0.003 STEEL 0.0008 F&F 0.0024		11.0°
⑩	.550	0.035 GLASS 0.0020 0.003 STEEL 0.0008 } 0.0052 F&F 0.0024		[illegible].1°
⑪	.980	0.034 GLASS 0.0019 0.003 STEEL 0.0008 } 0.0051 F&F 0.0024		- [illegible].0°

TABLE V

SECTION PROPERTIES

Section	r/R	I_f, in^4	I_c, in^4	J, in^4	EI_f, $lb - in^2$	EI_c	G J
① – ②	.091 - .113	17.8 X 10^3	6.80 X 10^3	24.6 X 10^3	516 X 10^3	197 X 10^3	270 X 10^3
② – ③	.142 - .145	2.60 X 10^3	3.61 X 10^3	6.2 X 10^3	75.4 X 10^3	105 X 10^3	68.1 X 10^3
③ – ④	.160 - .163	2.60 X 10^3	3.61 X 10^3	6.2 X 10^3	75.4 X 10^3	105 X 10^3	68.1 X 10^3
④ – ⑤	.195 - .198	0.84 X 10^3	2.93 X 10^3	3.8 X 10^3	24.2 X 10^3	86.0 X 10^3	41.8 X 10^3
⑤ – ⑥	.225 - .228	0.71 X 10^3	4.87 X 10^3	5.6 X 10^3	20.6 X 10^3	141 X 10^3	61.5 X 10^3

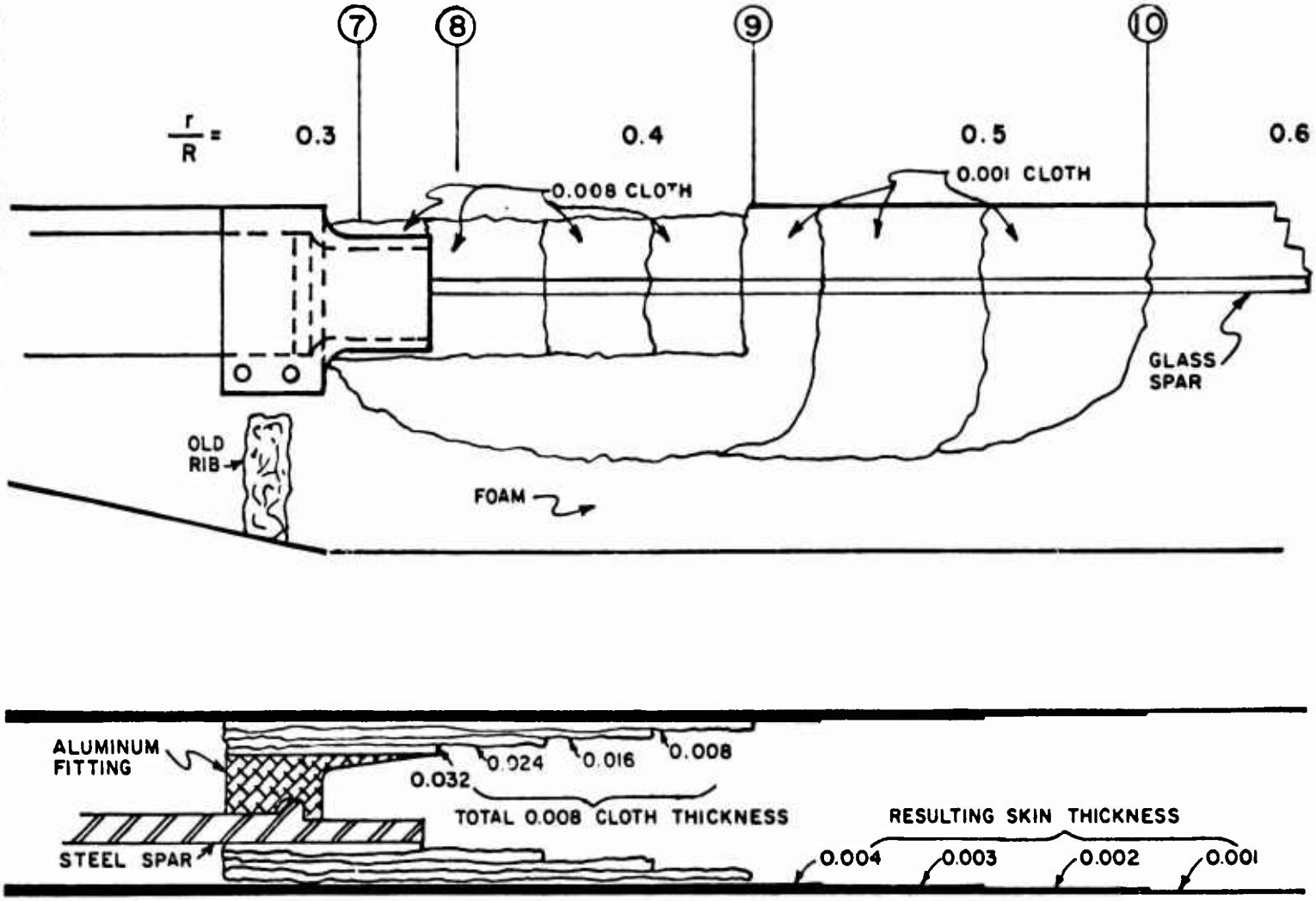

Aluminum fitting was made as a custom fit to slide over the steel spar from the trailing edge aft and was then riveted aft of spar. Entire assembly was chemically cleaned after sandblasting and assembled in a rapid time sequence of (1) epoxy bonding fitting to spar, (2) riveting before epoxy set-up and (3) epoxy-bond glass to root fitting and spar.

Figure 1. Revised Analysis Sections.

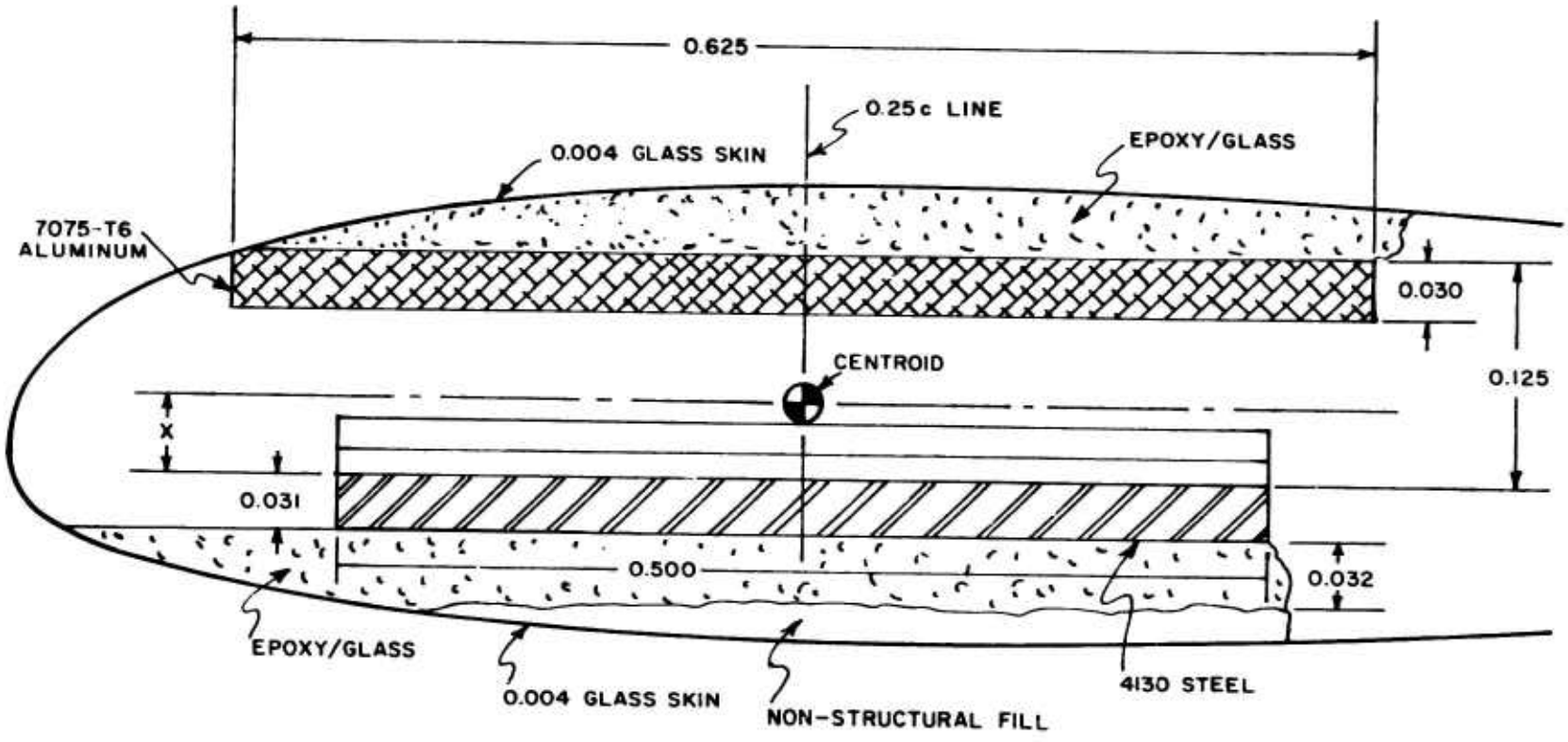

Figure 2. Section 7 - Structural Arrangement.

Section 7--Stiffness

Flapwise

Centroid determination: (considering steel and aluminum only)

$$(.125 - .015 - X)(.625 \times .031)10.3 \times 10^6 = (X + .015)(.5 \times .031) \times 29 \times 10^6$$

$$(.11 - X)(6.45) \quad 14.5 = X + .015$$

$$.049 - .445\,X = X + .015,\ 1.445\,X = .034,\ X = .024$$

$$I_{steel} = \frac{.5}{12}(.031)^3 + (.024 + .015)^2(.031 \times .5) = 25.8 \times 10^{-6}\,in^4$$

$$I_{aluminum} = \frac{.625}{12}(.030)^3 + (.125 - .024 - .015)^2(.030 \times .625) = 140 \times 10^{-6}\,in^4$$

$$I_{glass} = \frac{(.55 + .4)}{12}(.032)^3 + [(.024 + .031 + .016)^2 + (.125 - .024 + .016)^2](.55 + .4) \times .032$$

$$= [26 + (50.5 + 137)(3.04)] \times 10^{-6}$$

$$= 596 \times 10^{-6}\,in^4 + \underset{\substack{\downarrow \\ .004\ skin}}{97} \times 10^{-6} = 693 \times 10^{-6}\,in^4$$

(Flapwise and Radial)

$E_{steel_1} = 29 \times 10^6 psi$

$E_{aluminum_1} = 10.3 \times 10^6 psi$

$E_{glass_2} = 2.68 \times 10^6 psi$

$Area_{steel} = .016\ in^2$

$A_{aluminum} = .019\ in$

$A_{glass} = .030 + .015$ skin

$= .045$

$EI_{steel} = 1010\ lb\text{-}in^2$

$EI_{alum.} = 1440\ lb\text{-}in^2$

$EI_{glass} = 1850\ lb\text{-}in^2$

$\Sigma EI = 4300\ lb\text{-}in^2$

$EA_{steel} = 464 \times 10^3\ lb\text{-}in^2$

$EA_{alum.} = 196 \times 10^3\ lb\text{-}in^2$

$EA_{glass} = 121 \times 10^3\ lb\text{-}in^2$

$\Sigma EA = 781 \times 10^3\ lb\text{-}in^2$

Section 7--Stiffness (cont.)

Chordwise

$$I_{steel} = \frac{.031\ (.5)^3}{12} = 323 \times 10^{-6}\ in^4$$

$$I_{aluminum} = \frac{.030\ (.625)^3}{12} = 612 \times 10^{-6} in^4$$

$$I_{glass} = \frac{.032\ (.47)^3}{12} + \frac{.008\ (1.9)^3}{12} + (.47)^2\ (3.8 \times .004)$$

$$= 280 \times 10^{-6} + 4600 \times 10^{-6} + 3370 \times 10^{-6} = 8250 \times 10^{-6} in^4$$

$EI = 22{,}100$

$EI_{steel} = 9370\ lb\text{-}in^2$

$EI_{alum.} = 6300\ lb\text{-}in^2$

$EI_{glass} = 2250\ lb\text{-}in^2$

$\Sigma EI = 17{,}920\ lb\text{-}in^2$

Let us not consider these as applicable at this station due to lack of load path; instead use

$$2 \times \frac{.004}{12}\ (.94)^3 = 560 \times 10^{-6} in^4$$

$I_{glass} = 840 \times 10^{-6} in^4$

$EI = 2250\ lb\text{-}in^2$

1. MIL-HDBK 5, March 1961
2. From tests performed by WFP Company on .094 x .96 rectangular specimen and confirmed with tests on NACA 0015 airfoil section covered with .003 cloth.

Torsion

$G_{steel_1} = 11.0 \times 10^6 psi$

$G_{alum._1} = 3.9 \times 10^6 psi$

$G_{glass_3} = 1 \times 10^6$

$$GJ_{steel} = (1010 + 9370)\ \frac{11.0}{29.0} = 3{,}930\ lb\text{-}in^2$$

$$GJ_{aluminum} = (1440 + 6300)\ \frac{3.9}{10.3} = 2{,}040\ lb\text{-}in^2$$

$$GJ_{glass} = (1850 + 2250)\ \frac{1}{2.68} = 1{,}530\ lb\text{-}in^2$$

$\Sigma GJ = 7{,}500\ lb\text{-}in^2$

10 Hour Life
3p @1800 rpm
for 10 hr = 3.2×10^6 cycles

TABLE VI

MATERIAL STRESSES

COMPONENT	STEADY		ALTERNATING			ALLOWABLE
	TENSILE	SHEAR	FLAPWISE	CHORDWISE	TOTAL, psi	for 3.2×10^6 cycles
STEEL	4100 psi	YG=2.87×10^6 845 psi	YE=$.90\times10^6$ 2080 psi	YE=7.25×10^6 2440 psi	4520	40,000 psi [1]
ALUMINUM	1450 psi	YG=1.25×10^6 394 psi	YE=1.29×10^6 3000 psi	YE=3.22×10^6 1080 psi	4080	12,500 psi [1]
GLASS	378 psi	YG=$.47\times10^6$ 138 psi	YE=$.415\times10^6$ 960 psi	YE=1.26×10^6 423 psi	1383	15,000 psi [4]
TOTAL $\frac{T}{\sum EA}$ or $\frac{M}{\sum EI}$	$.141\times10^{-3}$	$.294\times10^{-3}$	2.32×10^{-3}	$.336\times10^{-3}$		

$$f_{t_x} = E_x \cdot \frac{T}{\Sigma EA} \quad , \quad f_{b_x} = Y_x E_x \frac{M}{\Sigma EI}$$

Aluminum is 7075 - T6

Steel is 4130 heat treated to 180,000 psi yield.

3. Poisson's Ratio, μ , assumed at a mid-value $\mu = 0.29$ and E computed from

$$G = \frac{E}{2(1+\mu)} = \frac{2.68 \times 10^6}{2.58} = 1.04 \times 10^6$$

1. MIL-HDBK-5 2.3.1.(2) and 3.3.1(c)

4. Undocumented number subject to approval and/or revision.

Section 8 STIFFNESSES

Flapwise--Glass Only

$$I_{flap} = I_{spar} + I_{.008\ cloth} + I_{.004\ skin}$$

$$= 55 \times 10^{-6} + 438 \times 10^{-6} + 97 \times 10^{-6}$$

$$I_{flap} = 590 \times 10^{-6}\ in^4$$

$$EI_{flap} = 1580\ lb\text{-}in^2$$

Chordwise--Glass Only

$$I_{chord} = [106 + 280 + 420 + 2000] \times 10^{-6}\ in^4$$

($.003$ skin, $.001$ skin)

$$I_{chord} = 2806 \times 10^{-6}\ in^4$$

$$EI_{chord} = 7{,}800\ lb\text{-}in^2$$

Torsion

$$J = 590 + 2806 = 3396 \times 10^{-6}\ in^4$$

$$GJ = 3{,}540\ lb\text{-}in^2$$

$$\text{Area} = (.95 \times .032)_{.031\ spar} + .026 + .004 + .006 = .067\ in^2$$

TABLE VII

SECTION 8 - STRESSES (GLASS)				
STEADY		ALTERNATING		
Tensile	Shear	Flap	Chord	Total
CF = 100	My = 2.93	My = 1.42	My = 1.42	
1,500psi	865psi	2,400psi	2,840psi	5,240psi

Section 9 STIFFNESSES

Flapwise--Glass Only

$$I_{flap} = I_{spar} + I_{skin\ .004"} = 54.3 \times 10^{-6} + 97 \times 10^{-6}\ in^4$$

$$I_{flap} = 151 \times 10^{-6}\ in^4$$

$$EI_{flap} = 390\ lb\text{-}in^2$$

Chordwise

$$I_{chord} = I_{spar} + I_{skin} = 104 \times 10^{-6} + (420 + 2000) \times 10^{-6}$$

for .003 partial; for .001 complete

$$= 2524 \times 10^{-6}\ in^4$$

$$EI_{chord} = 6{,}750\ lb\text{-}in^2$$

Torsion

$$GJ = (6750 + 390)\ \frac{1}{2.58} = 2{,}770\ lb\text{-}in^2$$

$$J = 2670 \times 10^{-6}$$

Area

$$A = A_{spar} = A_{.001\ skin} + A_{.003\ partial\ skin}$$

$$+ .026 + .004 + .006 = .036\ in^2$$

TABLE VIII

SECTION 9 - STRESSES (GLASS)				
STEADY		ALTERNATING		
Tensile	Shear	Flap	Chord	Total
	y = 1.4"	y = .15	y = 1.4	
2,780	945 psi	8,150	3,180 psi	11,330 psi
		My = 1.23	My = 8.0	

Section 10 STIFFNESSES

Flapwise--Glass Only

$$I_{flap} = (50 + 20) \times 10^{-6}$$

spar .001
skin

$$I_{flap} = 70 \times 10^{-6} \text{ in}^4$$

$$EI_{flap} = 188 \text{ lb-in}^2$$

Chordwise

$$I_{chord} = 2100 \times 10^{-6} \text{ in}^4$$

$$EI_{chord} = 5{,}620 \text{ lb-in}^2$$

Torsion

$$J = 2170 \times 10^{-6} \text{ in}^4$$

$$GJ = 2260 \times \text{lb-in}^2$$

Area = .035 in^2

TABLE IX

SECTION 10 - STRESSES (GLASS)				
STEADY		ALTERNATING		
Tensile	Shear	Flap	Chord	
CF = 70	y = 1.4 My = 1.26	y = 1.3 My = .84	y = 1.4 My = 5.4	Total
2,000 psi	900 psi	12,000 psi	2,570	14,570 psi

TABLE X

STEADY AND ALTERNATING STRESSES - SECTION 7 TO 10

SECTION	MATERIAL	I_f $\times 10^{-6}$ in^4	I_c $\times 10^{-6}$ in^4	EI_f lb-in^2	EI_c lb-in^2	GJ lb-in^2	STRESSES					
							STEADY		ALTERNATING			ALLOWABLE for 3.2×10^6 cycles
							TENSILE psi f_t	SHEAR psi f_s	FLAPWISE psi f_b	CHORDWISE psi f_b	TOTAL, psi f_b	
7	STEEL	25.8	323	1010	9370	3930	4100	YG=2.87X10^6 845	YE=.90X10^6 2080	YE=7.25X10^6 2440	4520	40,000
	ALUMINUM	140	612	1440	6300	2040	1450	YG=1.25X10^6 394	YE=1.29X10^6 3000	YE=3.22X10^6 1080	4080	12,500
	GLASS	693	840	1850	2250	1530	378	YG=.47X10^6 138	YE=.415X10^6 960	YE=1.26X10^6 423	1383	15,000
8	GLASS	590	2806	1580	7800	3540	CF=100 1500	M_y = 2.93 865	M_y=1.42 2400	M_y = 8.0 2840	5240	
9	GLASS	151	2524	390	6750	2770	2780	y=1.4" 945	y=.15 M_y=1.23 8150	y=1.4 M_y =8.0 3180	11,330	15,000
10	GLASS	70	2100	188	5620	2260	CF=70 2000	y=1.4 M_y =1.96 900	y=.13 M_y=.84 12,000	y=1.4 M_y=5.4 2570	14,570	

$$f_{t_i} = E_i \frac{T}{\Sigma EA} \qquad f_{b_i} = Y_i E_i \frac{M}{\Sigma EI}$$

Section 11

$I_{FLAP} = 51 \times 10^{-6}$

$EI_{FLAP} = 137$ lb-in^2

$I_{CHORD} = 2100 \times 10^{-6}$

$EI_{CHORD} = 5630$ lb-in^2

$J = 2151 \times 10^{-6}$

$GJ = 2240$ lb-in^2

Areas as computed are valid

SECTION III

BLADE BENCH TEST RESULTS

1. INTRODUCTION

The purpose of the bench test was to measure blade properties such as shear center, elastic coupling, flapping inertia, and weight.

2. BLADE DEFLECTION DATA

The data for obtaining the structured influence coefficients were obtained by mounting the blades in the rotor hub, supporting the hub on a rigid base, and measuring the deflections at the 3/4 radius station due to loads applied at the blade tip. The apparatus used to perform these tests is pictured in Figures 3 through 6 and consisted of the following:

a. Bridgeport vertical milling machine

b. Aluminum target affixed to the blade 3/4 radius station

c. 1/8-inch diameter probe mounted in but insulated from the mill spindle

d. Battery and light bulb arrangement for indicating when the probe touched the target

e. Various pieces of aluminum bar, plate, and angle and assorted clamps and pulleys for load application

The test procedure was to locate the various reference surfaces on the target, shown in Figure 7, by moving the hub-blade-load system with respect to the probe by means of the three mutually perpendicular feeds of the milling machine. At no load, the various feed indices were set to zero when the probe touched the target. After application of a load, the blade system was relocated in a similar fashion and the corresponding feed indices were read and recorded, thus determining the blade deflection. A total of four readings was taken at each loading; vertical displacement (chordwise), horizontal displacement (flapwise), and two horizontal displacements 4.00 inches apart for determination of torsional deflection.

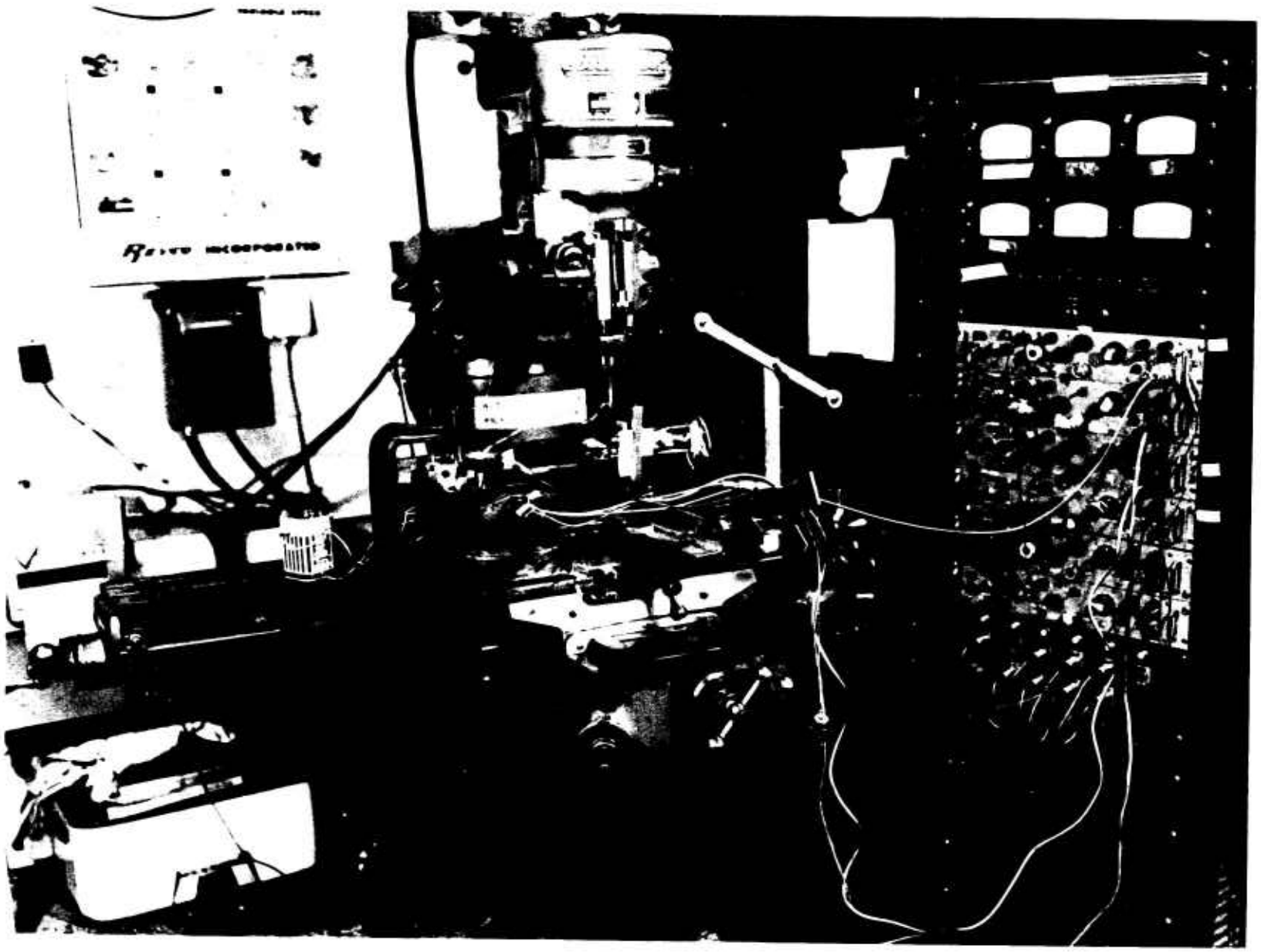

Figure 3. Test Setup To Obtain Blade Deflection Data

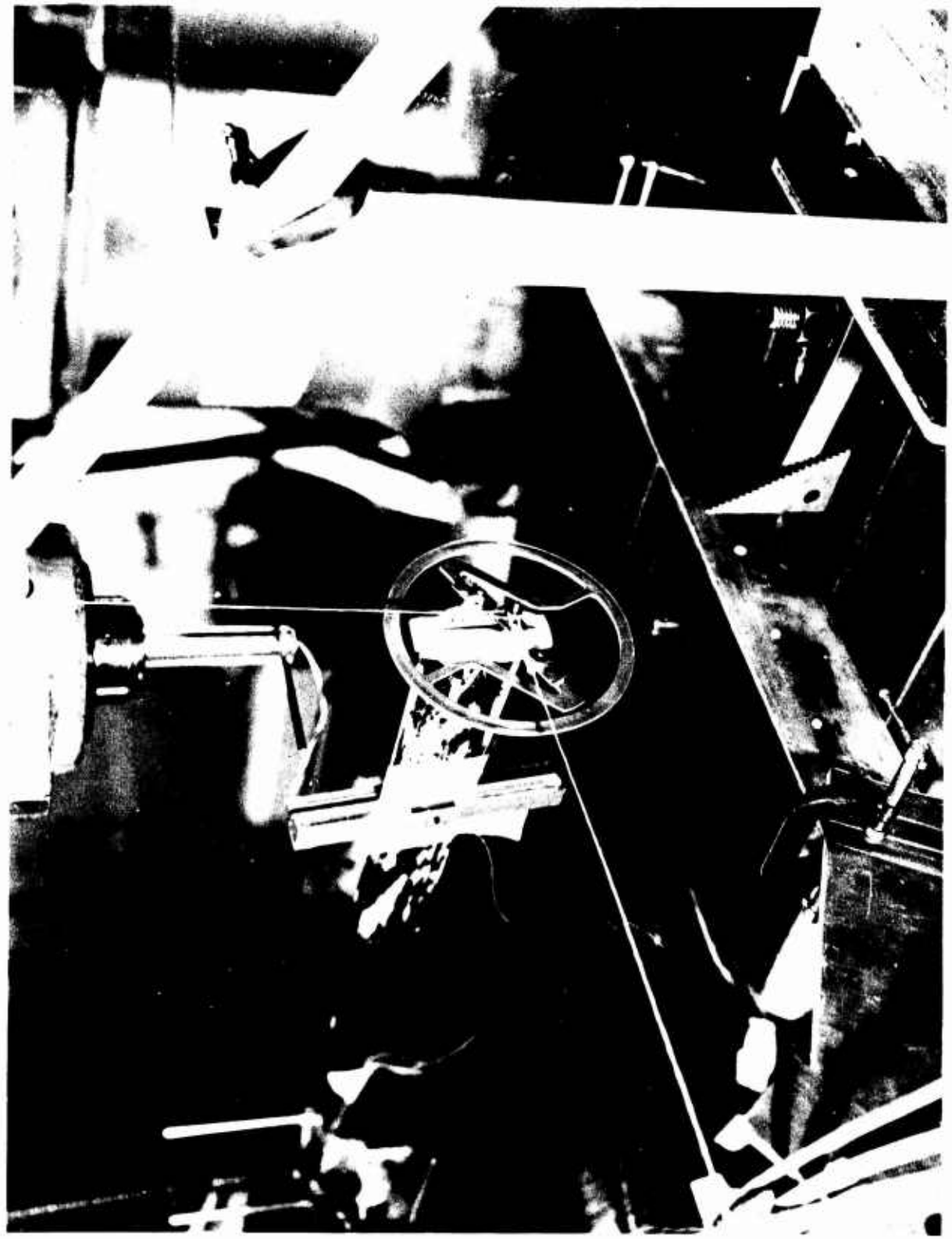

Figure 4. Load Application at Blade Tip.

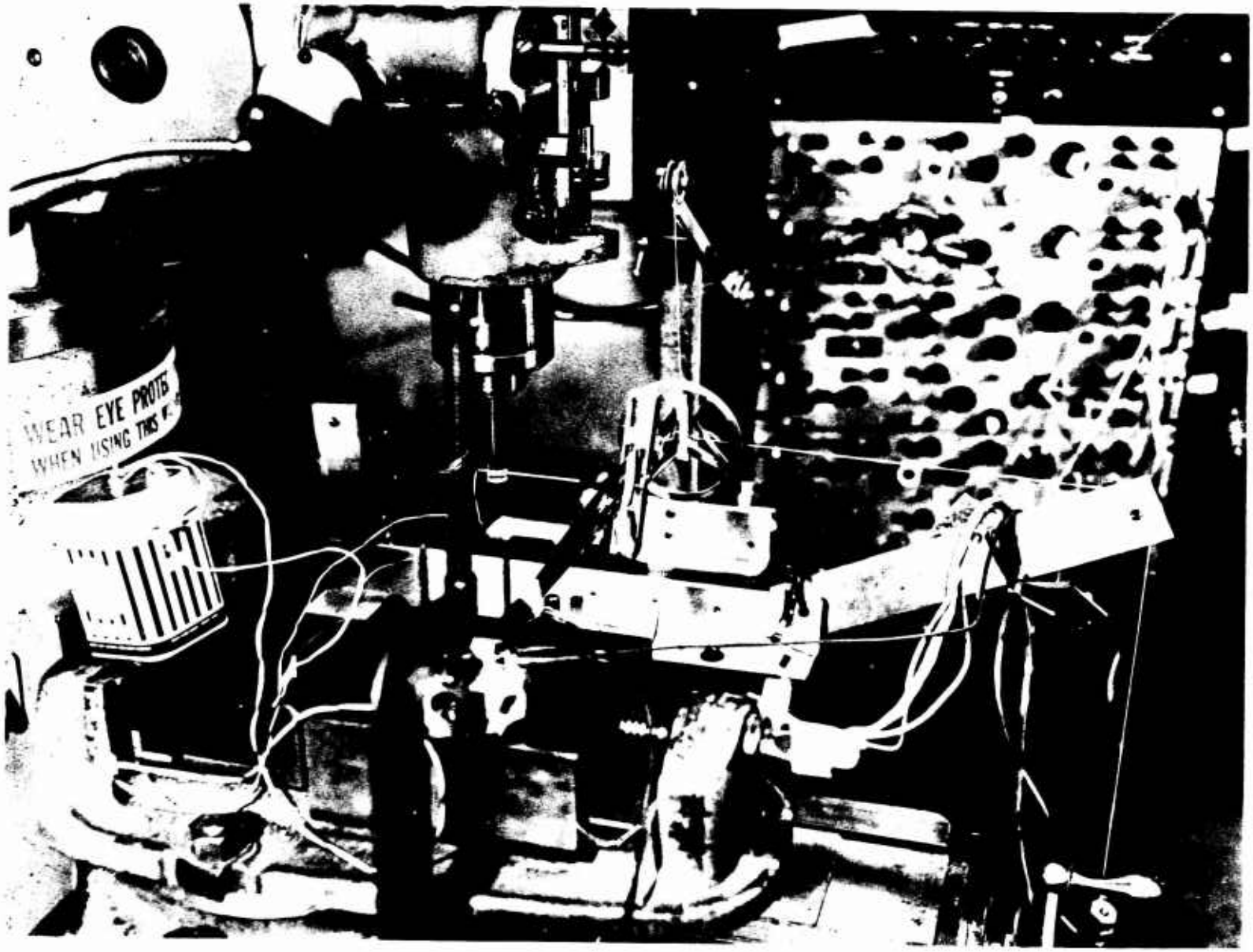

Figure 5. Blade Measurement at 3/4 Radius Station

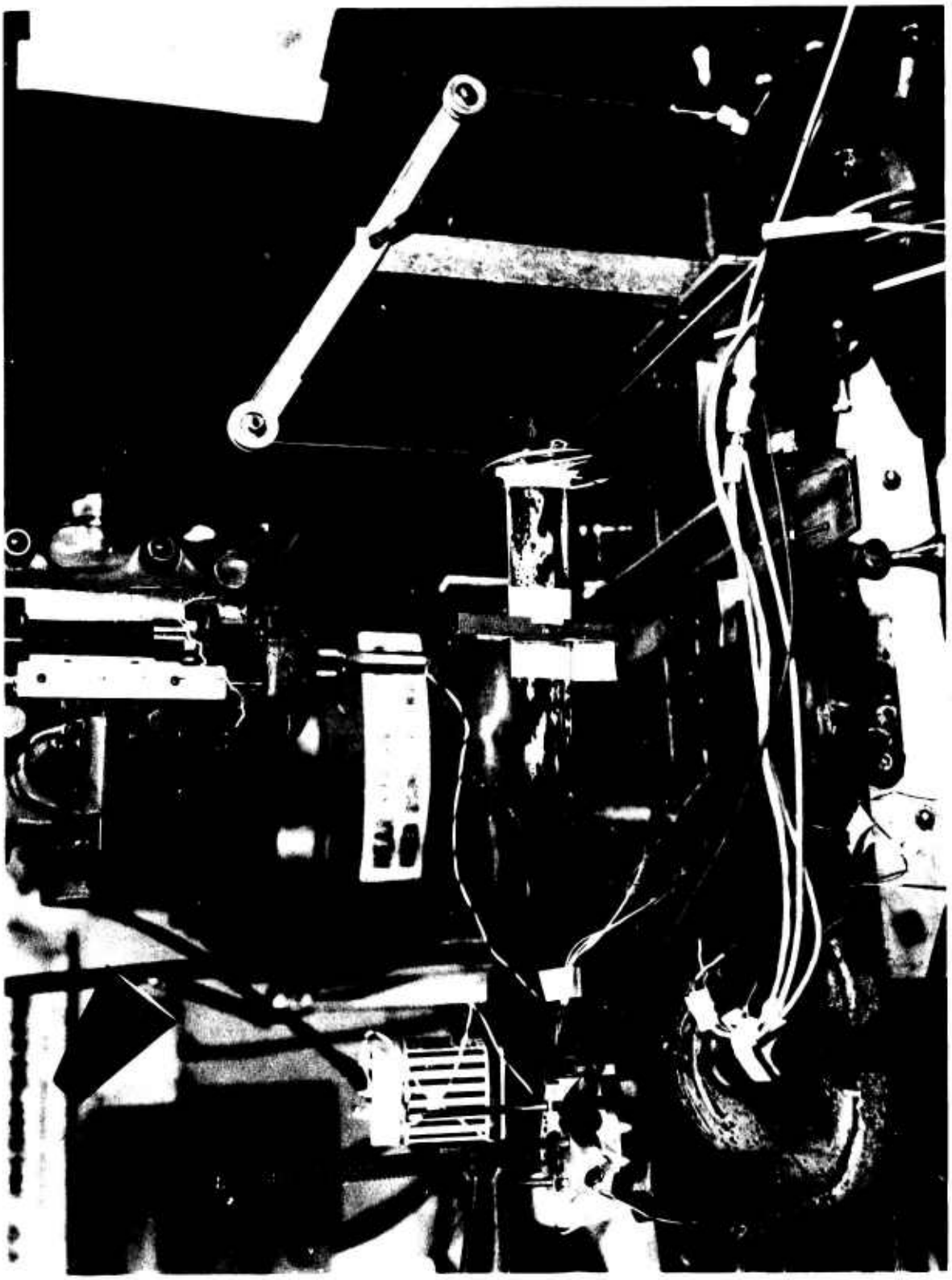

Figure 6. Blade Root and Hub Attachment.

Referring to Figure **7**, the flapwise displacement Δf can be expressed in terms of the horizontal feed displacement f as

$$\Delta f \cong f + 0.127 \quad \Delta\theta .$$

Similarly, the chordwise deflection ΔC can be expressed in terms of the vertical displacement C as

$$\Delta C \cong C + 0.369 \quad \Delta\theta .$$

Finally, the torsional deflection $\Delta\theta$ can be expressed in terms of ΔX, the difference in the two horizontal displacements taken 4.00" apart, as

$$\Delta\theta \cong \frac{\Delta X}{4.125 + 0.441 \quad \Delta X}$$

In all the above it has been assumed that $\Delta\theta$ is a small angle (less than 5°).

These corrections have been applied to the measured data and the resulting corrected data for the four blades tested are presented in **Table XI.**

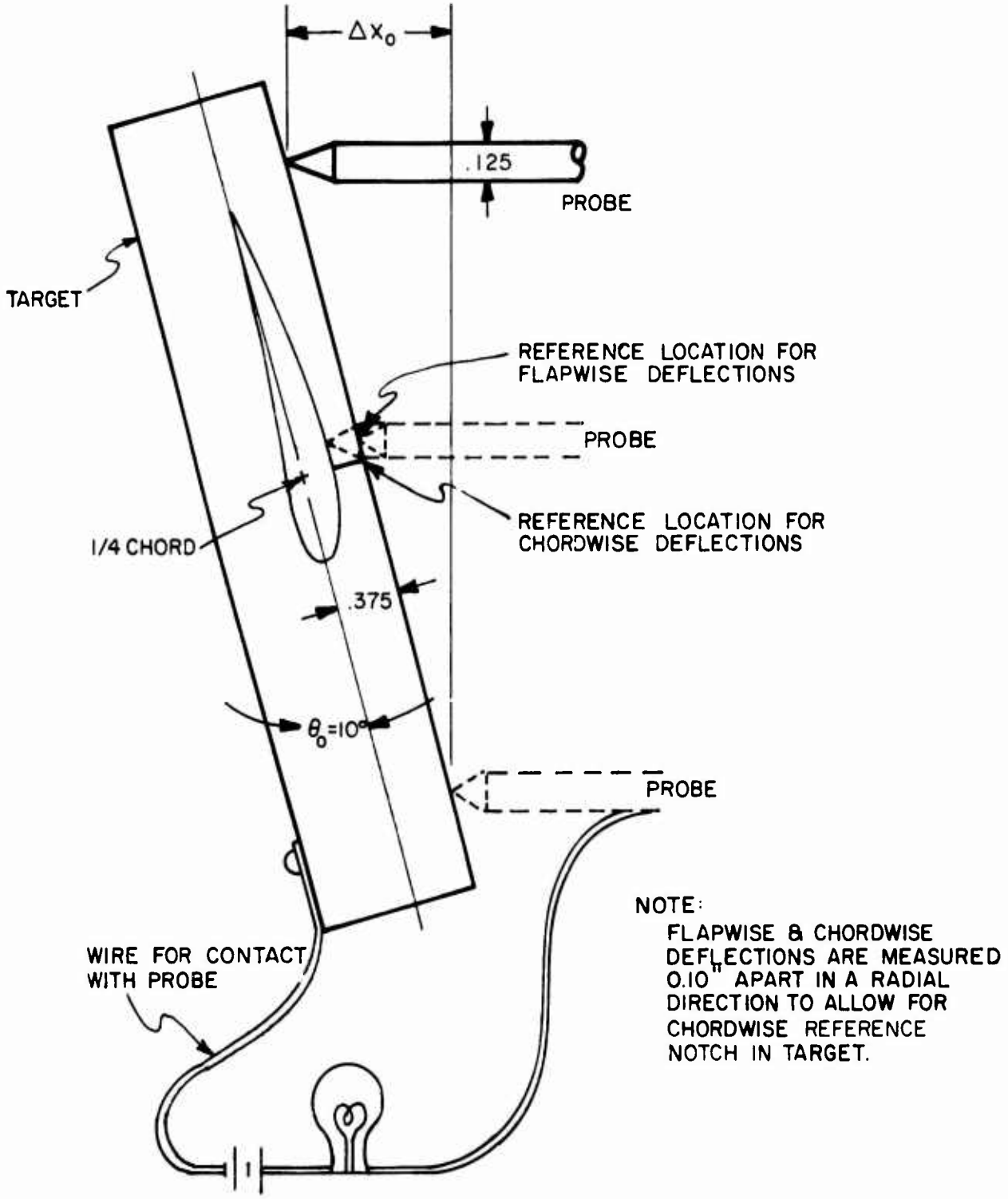

Figure 7. Setup to Obtain Reference Surfaces.

TABLE XI
BLADE TORSION AND DEFLECTION CORRECTIONS

APPLIED LOAD, lb.		BLADE 1 (BLUE)			BLADE 2 (YELLOW)			BLADE 3 (RED)			BLADE 4 (GREEN)		
F	C	$\Delta\theta°$	$\Delta f''_{.75R}$	$\Delta c''_{.75R}$	$\Delta\theta°$	$\Delta f''_{.75R}$	$\Delta c''_{.75R}$	$\Delta\theta°$	$\Delta f''_{.75R}$	$\Delta c''_{.75R}$	$\Delta\theta°$	$\Delta f''_{.75R}$	$\Delta c''_{.75R}$
.634	0	-.43	.840	-.255	-.46	.622	-.206	-.08	+.666	-.158	-.72	.816	-.254
.369	↓	-.52	.398	-.158	-.26	.381	-.119	-.15	.323	-.089	-.24	.485	-.159
0		0	0	0	0	0	0	0	0	0	0	0	0
-.369		-.10	-.500	+.168	+.03	-.372	.136	-.08	-.412	+.108	-.38	-.489	+.174
-.553		-.31	-.763	.239	-.42	-.571	.103	-.12	-.619	+.158	-1.02	-.739	.247
+.614	.061	-.87	+.796	-.233	-.71	.638	-.178	-.18	+.662	-.140	-.56	+.778	-.238
.614	.123	-.86	.779	-.180	-.46	.614	-.144	-.30	.647	-.117	-.83	.760	-.211
.369	.123	+.84	.550	-.096	-.17	.354	-.065	+1.15	.390	-.050	-.40	.446	-.102
.369	.184	-.49	.427	-.067	-.10	.337	-.029	.24	.381	-.034	-.40	.426	-.065
0	.246	+.24	-.101	.127	+.24	-.085	+.138	.18	-.064	+.111	+.32	-.104	.143
0	.369	.39	-.152	.191	.36	-.119	.200	.18	-.110	.154	.47	-.156	.212
-.369	.246	.54	-.603	.287	.22	-.472	.267	.29	-.472	.218	.28	-.586	.307
-.369	.369	.78	-.658	.347	.14	-.603	.323	.33	-.485	.268	.82	-.627	.374
-.614	.246	.29	-.937	.386	.21	-.728	.343	.15	-.725	.277	.06	-.922	.402
-.614	.369	1.00	-.982	.428	.49	-.771	.410	.28	-.753	.329	.14	-.957	.457
+.614	-.184	-.08	+.830	-.327	-.44	.682	-.292	-.28	+.665	-.224	-.12	.815	-.349
.614	-.307	+.42	.845	-.347	-1.03	.666	-.335	+.24	.681	-.262	+.25	.800	-.368
.369	-.246	-.01	.554	-.251	-.33	.436	-.238	.10	.450	-.189	.15	.523	-.259
.369	-.307	-.24	.567	-.277	-.21	.439	-.265	0	.455	-.211	.18	.530	-.293
0	-.246	-.22	.096	-.119	-.06	.069	-.125	-.06	.065	-.102	.06	.086	-.129
0	-.369	-.18	.127	-.161	-.21	.103	-.151	-.06	.091	-.158	-.83	.130	-.152
-.369	-.123	-.24	-.433	+.099	-.10	-.345	+.066	+.24	-.360	.056	-.40	-.426	+.109
-.369	-.184	-.26	-.423	.063	-.26	-.312	.044	-.15	-.337	.034	-.61	-.391	.064
-.614	-.061	-.51	-.796	.234	-.29	-.617	.183	-.22	-.636	.144	-.89	-.773	.223
-.614	-.123	-1.09	-.739	.184	-.64	-.592	.147	-.62	-.622	.117	-1.01	-.743	.199

LOADING DIAGRAM

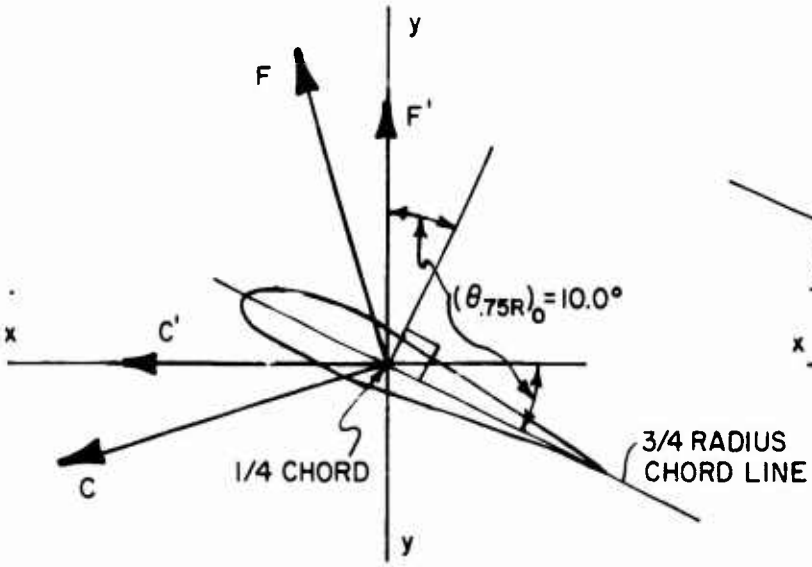

DEFLECTION DIAGRAM

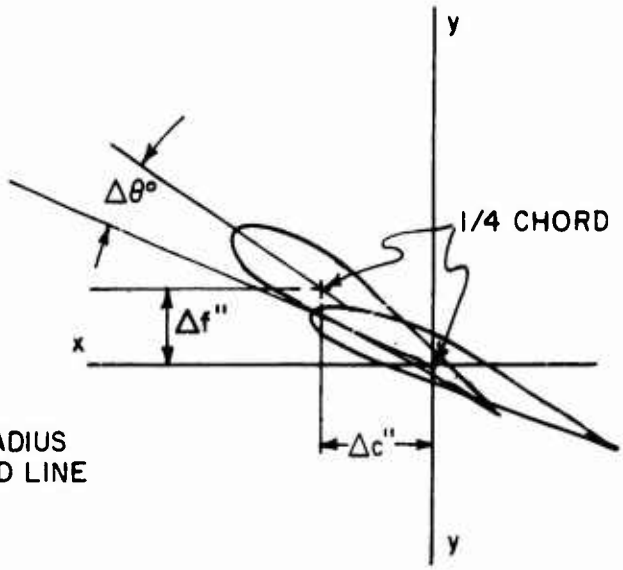

F = Applied flapwise load

(+ for tension in lower surface of blade)

C = Applied chordwise load

(+ for tension in trailing edge of blade)

F'= Flapwise load perpendicular to plane of rotation of rotor when $\theta_{.75R} = 10.0°$.

F' is measured along the space-fixed axis y-y. F' + for tension in blade lower surface.

C'= Chordwise load perpendicular to F'; measured along space-fixed axis x-x.

C' + for tension in blade trailing edge.

From the geometry of the load application arrangement it can be shown that:

$F' = F$ for $C > 0$

$F' = F + (0.21\ \Delta f'')\ C$ for $C < 0$

$C' = C - (0.138\ \Delta c'')\ F$ for $F > 0$

$C' = C - (0.102\ \Delta c'')\ F$ for $F \leq 0$.

The above formulae were obtained from the load application geometry depicted below and shown in the photographs of Figures 3 through 6.

LOAD APPLICATION GEOMETRY

Load Applied 0.22" beyond tip

$r = 16.875 + 0.22$

$= 17.10"$

$$\left.\frac{\delta_{tip}}{\delta_{.75R}}\right|_{chordwise} = 1.48$$

$$\left.\frac{\delta_{tip}}{\delta_{.75R}}\right|_{flapwise} = 1.68$$

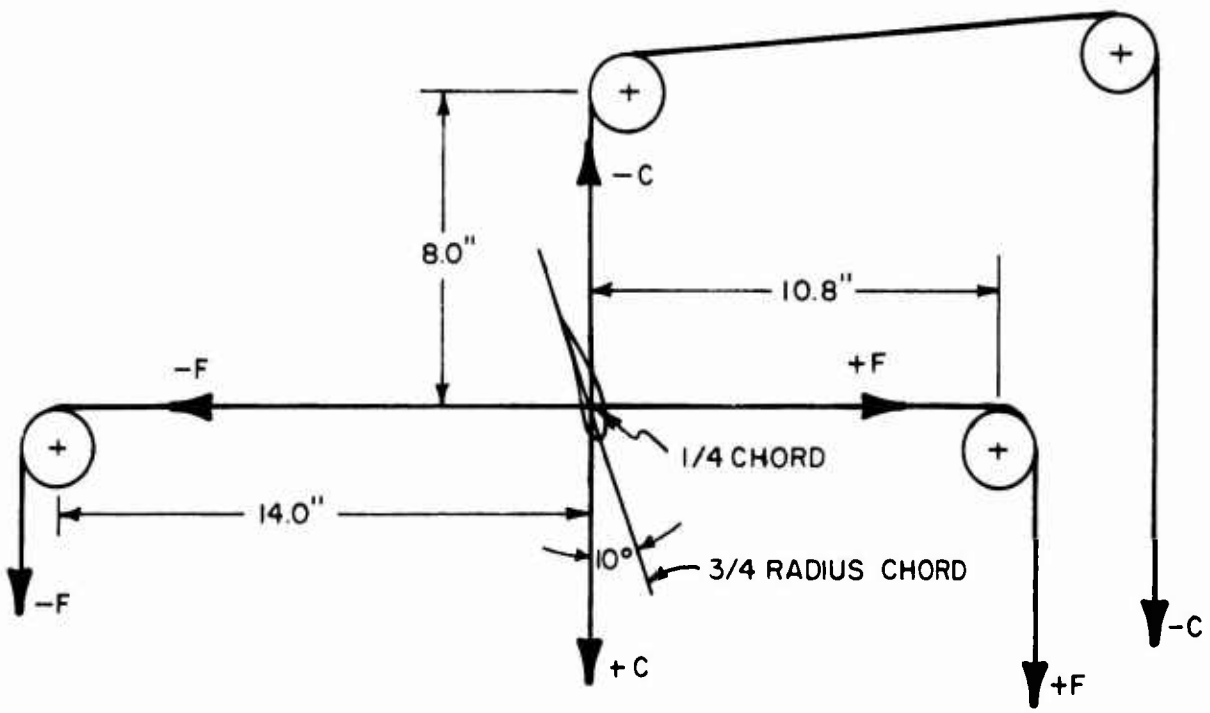

For computation of tip deflection as function of 3/4 R deflection a virtual hinge at $\frac{r}{R} = 0.17$ for chordwise bending is assumed while for flapwise bending the blade is treated as a uniform cantilever beam.

3. ERROR EVALUATION

The basic deflection measurement system allowed accuracies of ±.005" thus giving f and c to this accuracy and $\Delta\theta$ to an accuracy of $\pm. \frac{005}{4} \times 57.3 = \pm.07^\circ$.

The target-probe geometry was also accurate to within ±.005", which when combined with the small values of $\Delta\theta$, produces a negligible contribution to inaccuracy thus giving commensurate accuracy of ±.005" to the corrected values of Δf"and Δc". The overall accuracy of Δf and Δc are thus approximately $\frac{1}{3}\%$ and 1% respectively of their full scale values.

A systematic error was involved in the location of the flapwise and chordwise reference points on the target, with the chordwise measurements taken at a point 0.10" farther towards the tip of the blade than the 3/4 R station (where the flapwise reference point was located). Assuming a virtual hinge at $\frac{r}{R} = 0.17$ this produced a systematic error of $\epsilon = \frac{.10}{(.75-.17)} \times \frac{1}{16.87} \Delta c$ in the measurement of Δc or $\epsilon = .011\ \Delta c$. This produces a 1% error in the tabulated values of Δc which has not been corrected.

Load application point was accurate to ± .05" which is equivalent to 0.3% Radius.

The load application geometry was measured to an accuracy of ±.25". For the worst case of C<0

$$C' = C - [(1 + \epsilon)\ (.138)\ \Delta c"]\ F, \quad \epsilon = \frac{.25}{10.8} = 0.23$$

$$= -.3 - [(1 + \epsilon)\ (.138 \times .3)].6 = -.3 - [(1 + \epsilon)\ (.025)]$$

thereby giving a 2% error in a 10% correction or a net error of 0.2%.

Another source of measurement error was in the non-standard weights used to load the blades. These weights consisted of common $\frac{1}{2}$ - 18 steel nuts which were calibrated on a precision Ohms balance (10 at a time) and were found to weigh an average of 27.9 grams each. The scale is accurate to within 1 gram and therefore any systematic error is less than 1 out of 279 (for 10 nuts) or 0.3%. Individual nuts appeared to weigh identically within the sensitivity of the scale which is approximately $\pm\frac{1}{2}$ gram. This allows a possible random error of $\pm 1.5\%$ in the individual load values.

The remaining source of error, and probably the principal one, is that due to blade plastic creep. This error will be most apparent in flapwise deformations where the plastic carries a significant strain energy. Chordwise deformations occur mostly in the steel root fitting where creep is not significant. An attempt was made in performing the experiments to minimize the effects of plasticity by allowing the short-term transient to die out before measurements were taken. A typical time history of plastic deformation is shown below showing the deflection measured.

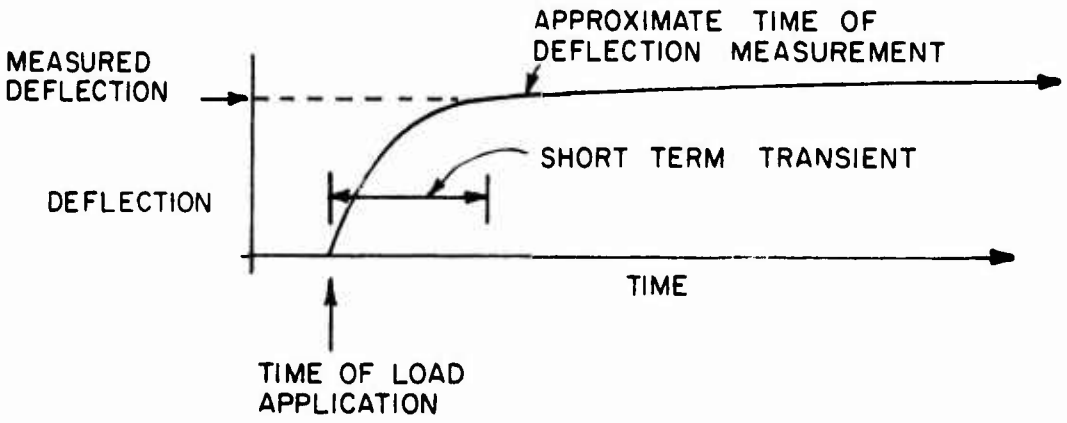

4. BLADE INERTIAS

Blade inertias were measured by means of swinging the blade as a compound pendulum about the center of rotation of the rotor. This was accomplished in the test set-up which consisted of

1.) a shaft supported on precision bearings (a size 8 servo motor was used),

2.) a root fitting attachment that allowed the shaft to support the blade by its root fitting with the rotational axis exactly at the equivalent rotor shaft center line, and

3.) a stop watch.

The procedure was as follows: with the blade supported at the rotor ℄ and taking care that instrumentation wires did not interfere with the blade swinging motion, the blade was set in motion and its period of motion was measured with the stop watch and recorded. Next, the blade weight and center of gravity were determined and recorded. From these two measurements the pendulcus spring rate was computed

$$K_\theta = r_{cg} \times W_{blade} \text{ for small oscillations.}$$

The inertia of the complete blade about the axis of rotation could then be determined from the expression $I = \frac{K_\theta}{(\frac{2\pi}{P})^2}$. A correction factor was then applied to obtain the inertia of that part of the blade outboard of the $\frac{r}{R} = 0.15$ station. This correction was computed analytically and was approximately 3% of the total number.

$I_{outboard} = I_{measured} - .0009 \cong .027$ slug-in^2 . The results of these experiments are presented in Table XII.

TABLE XII
BLADE INERTIA CHARACTERISTICS

Blade No.	Tip Color	Period, sec.	ω^2	r_{cg}"	W, gms*	K_θ, $\frac{\text{in-lb}}{\text{rad}}$	I_{meas} / lb-in-sec = slug-in^2	$I_{.15}$ / lb-in-sec = slug-in^2	W, gms†
1	Blue (Uninstrumented)	.987	40.5	5.75	91.5	1.13	.0281	.0272	98 gms
2	Yellow	.983	40.8	5.67	93.9	1.17	.0286	.0277	
3	Red	.985	40.8	5.65	94.8	1.18	.0288	.0279	100 gms
4	Green	.983	40.8	5.78	91	1.16	.0284	.0275	97 gms

* Weights are without pitch horn
† Weights with pitch horn

5. ERROR ANALYSIS

By far the most important source of error in the above experiments is due to the wire mass and spring constant on the instrumented blades. As much as ± 0.2 inch error in determining r_{cg} was possible from spring and blade weights could be in error by ± 5 gm. These two items alone give an uncertainty of

$$\pm\left(\frac{0.2}{5.7} + \frac{5}{92}\right) = \pm\ (0.035 + 0.055) = \pm\ 9\%$$

Any other errors are negligible compared to these.

The uninstrumented blade inertia is estimated to be accurate to within $\pm 3\%$ with accumulated errors of timing, r_{cg} measurement, and weighing.

6. ELASTIC COUPLING AND SHEAR DETERMINATION

The coupling between flap bending, chord bending moment, and torsional deflections resulting from bending is shown in Figures 8 through 10 for blade No. 4, Figures 12 through 14 for blade No. 1, Figures 16 through 18 for blade No. 2, and Figures 20 through 22 for blade No. 3. The shear center determination is shown in Figures 11, 15, 19, and 23 for blades No. 1, 4, 2 and 3, respectively. Corresponding blade deflection data are given in Tables XIII through XVI.

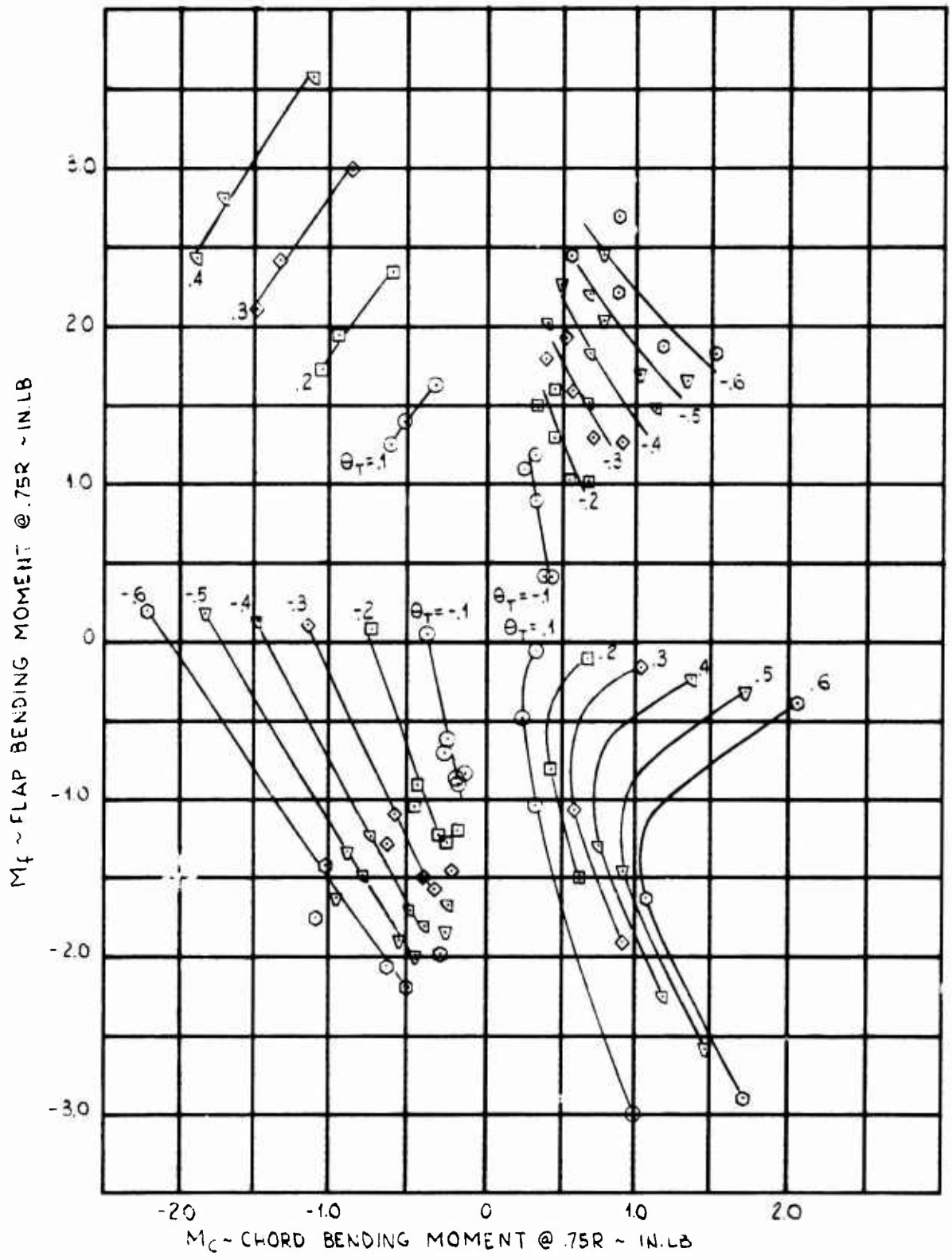

Figure 8. Blade No. 4 (Green) Deflection Data.

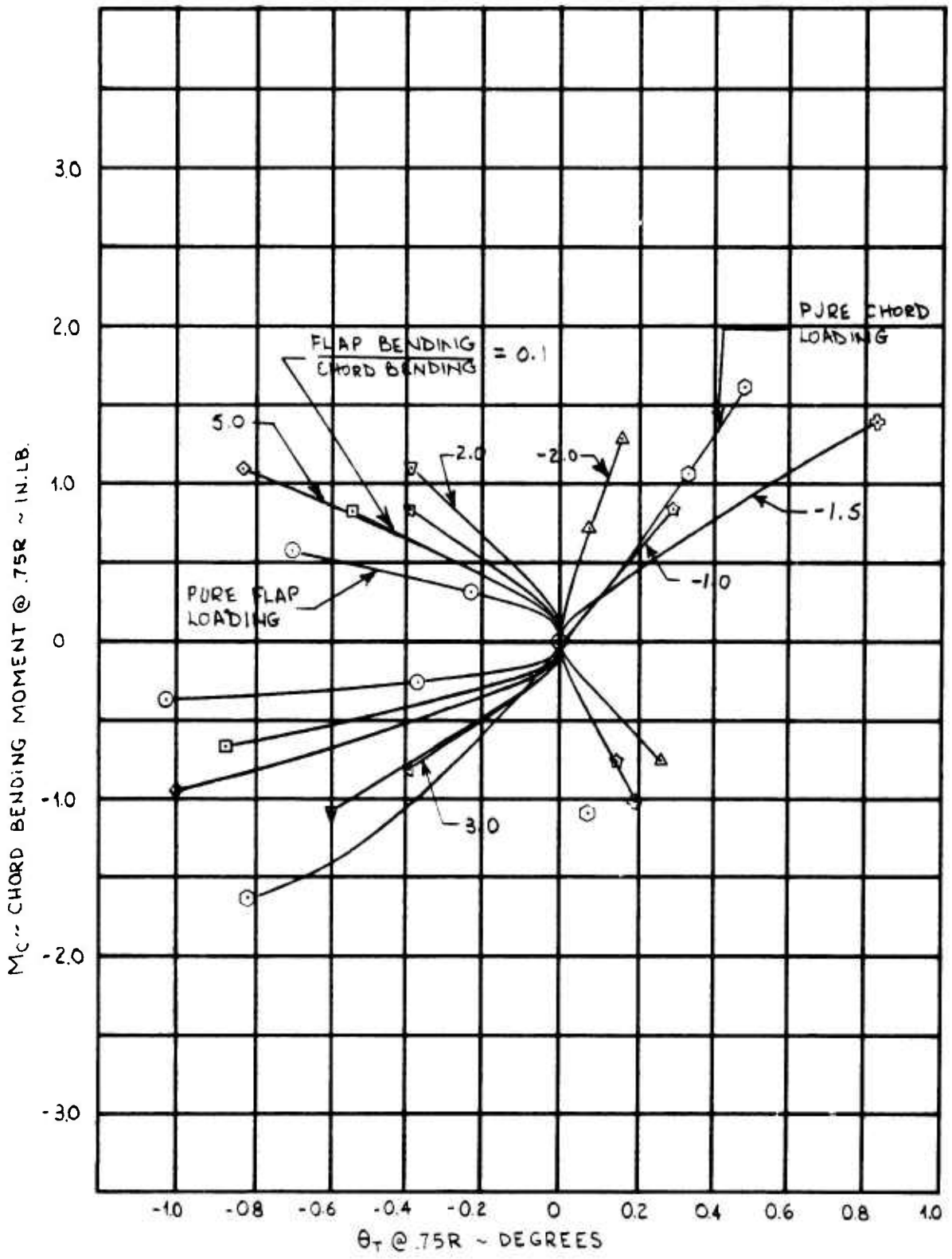

Figure 9. Blade No. 4 (Green) Deflection Data.

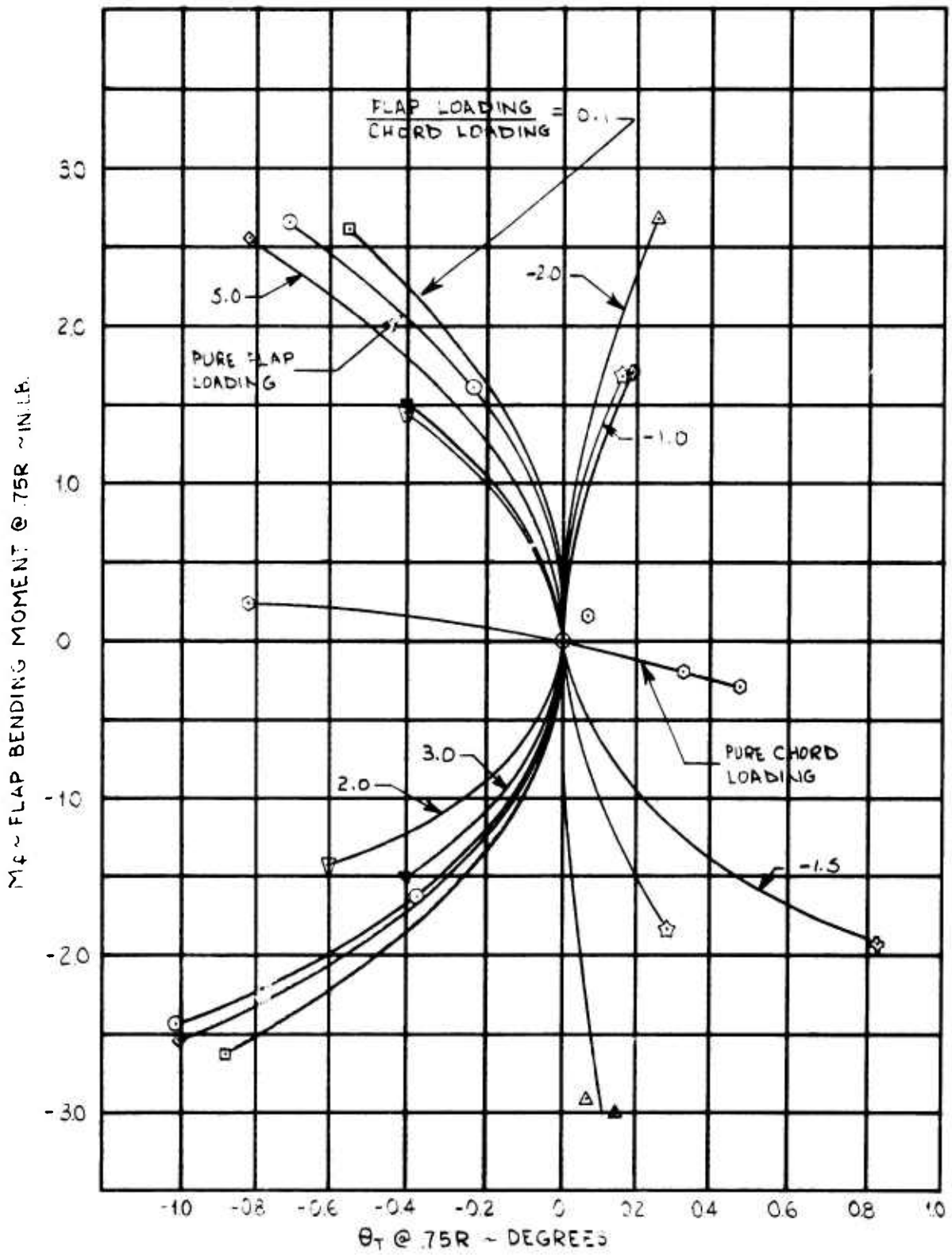

Figure 10. Blade No. 4 (Green) Deflection Data.

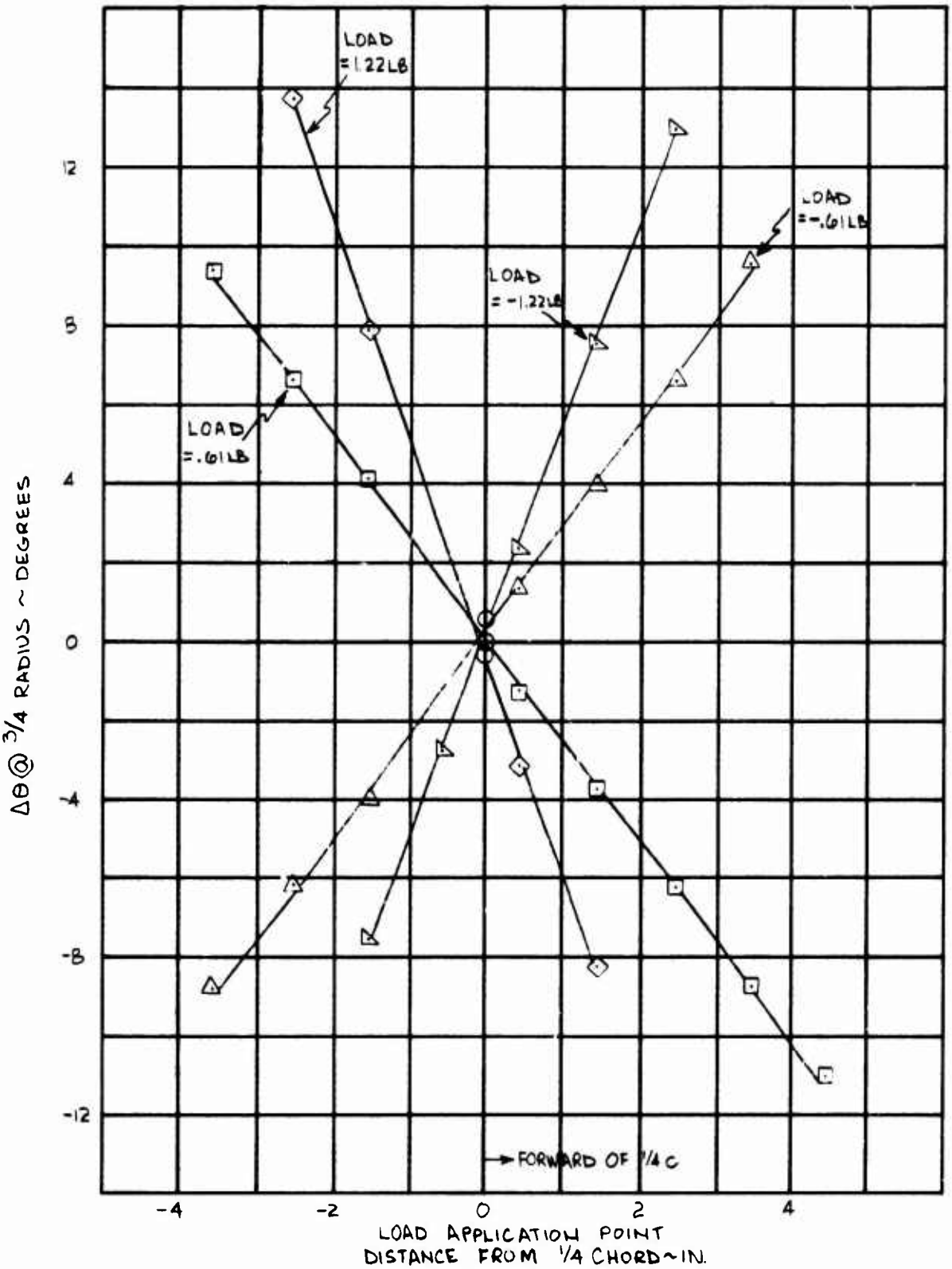

Figure 11. Blade No. 4 (Green) Shear Center Determination at 3/4 Radius.

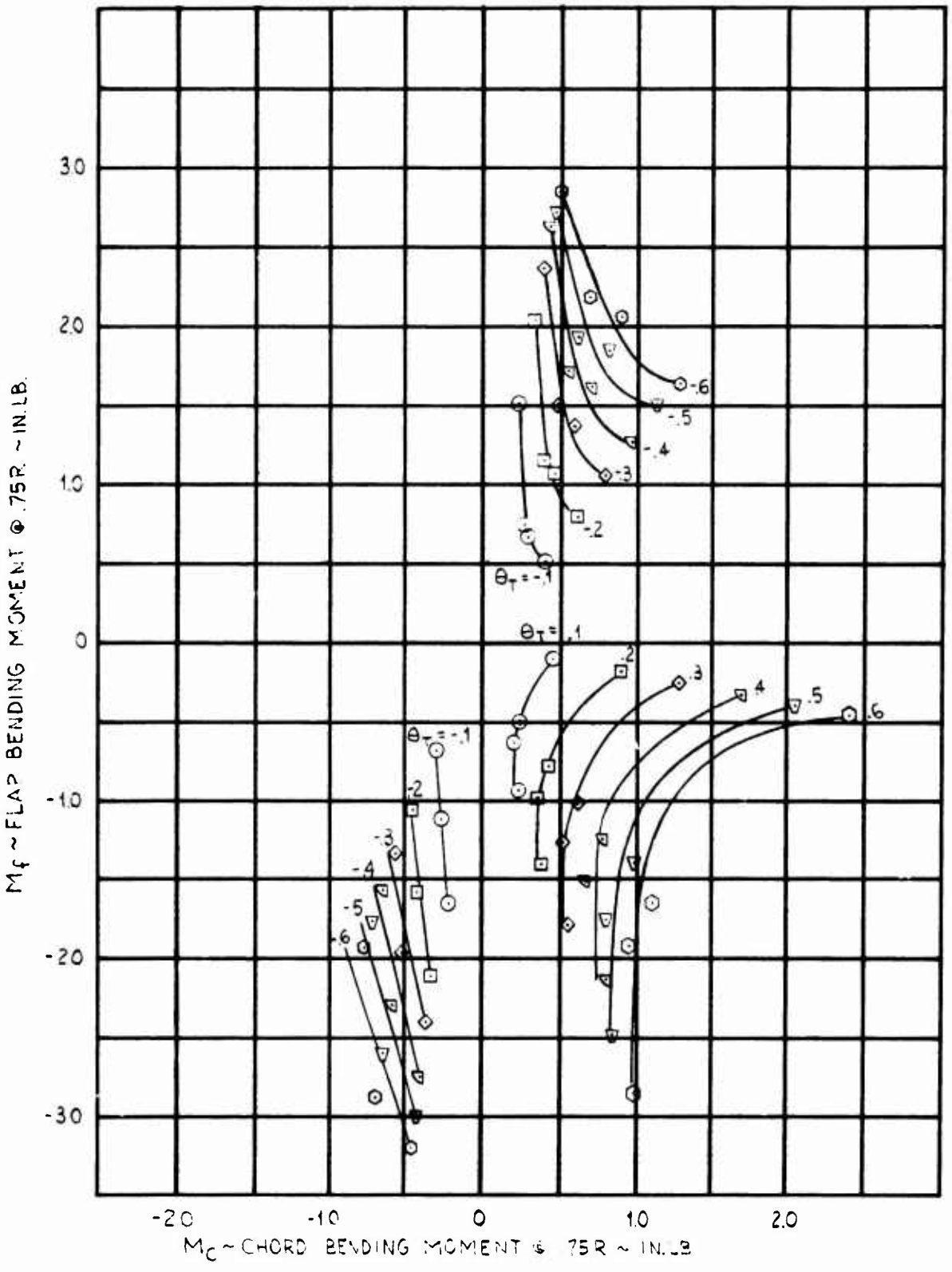

Figure 12. Blade No. 1 (Blue) Deflection Data.

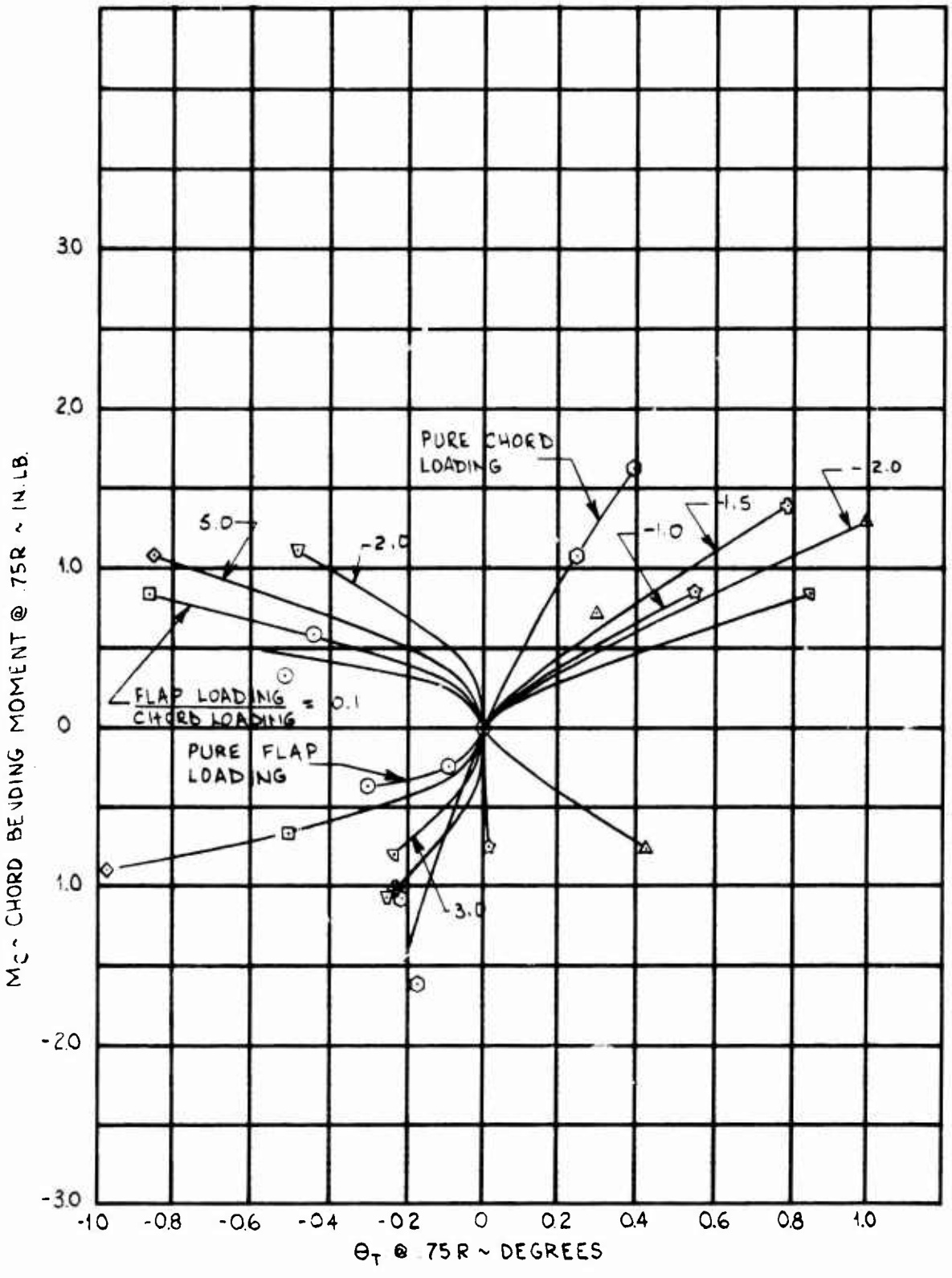

Figure 13. Blade No. 1 (Blue) Deflection Data.

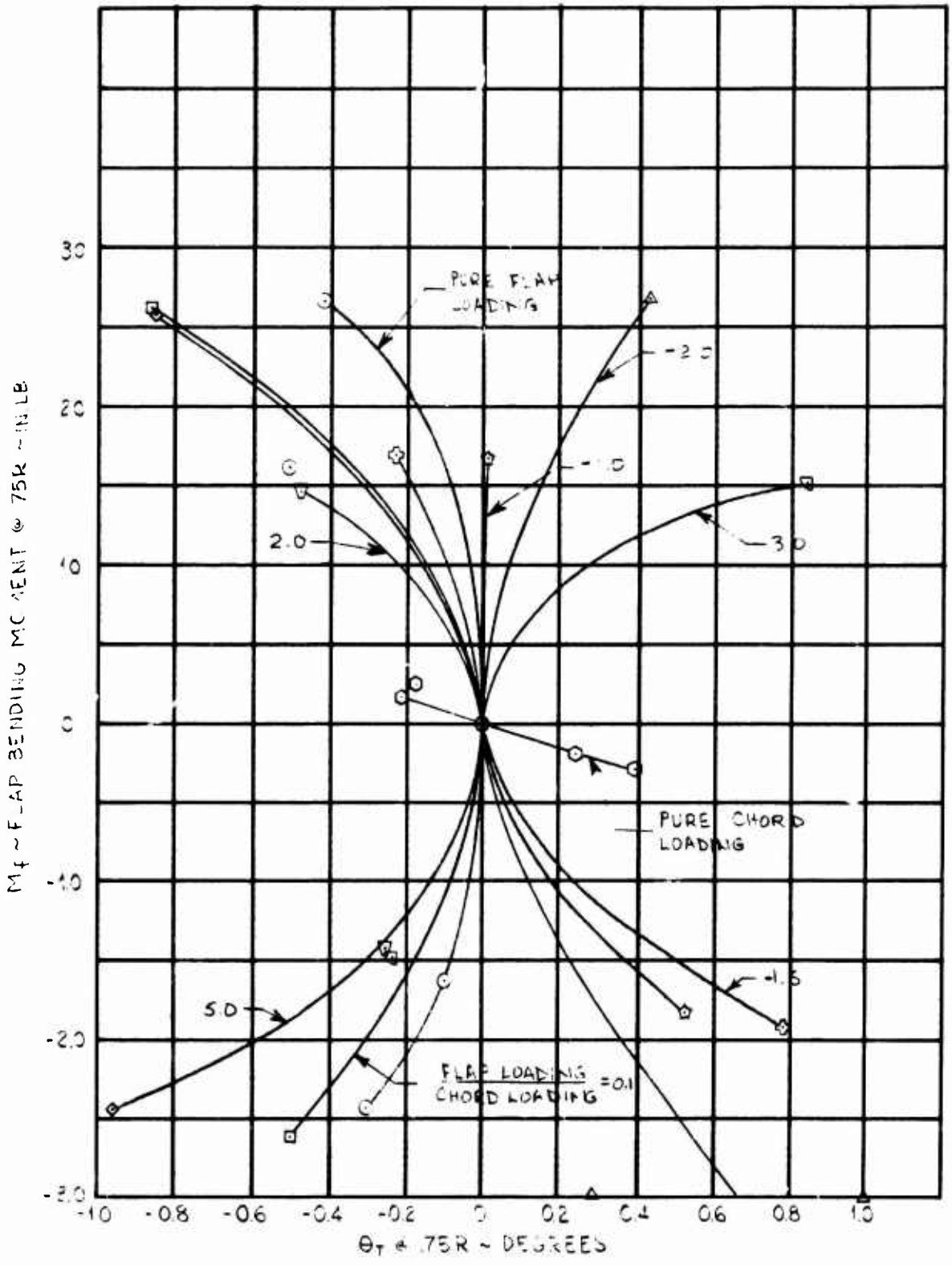

Figure 14. Blade No. 1 (Blue) Deflection Data.

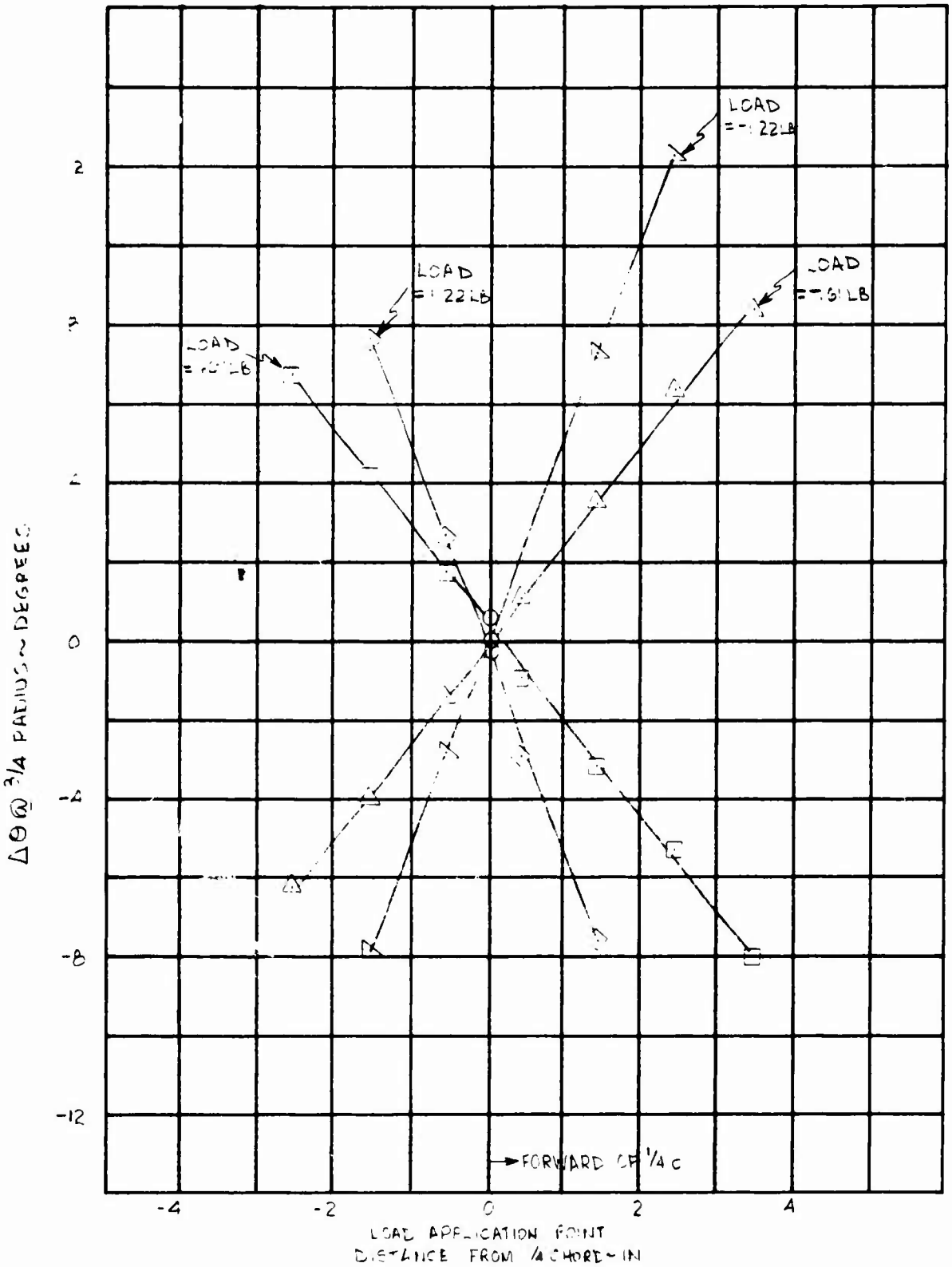

Figure 15. Blade No. 1 (Blue) Shear Center Determination at 3/4 Radius.

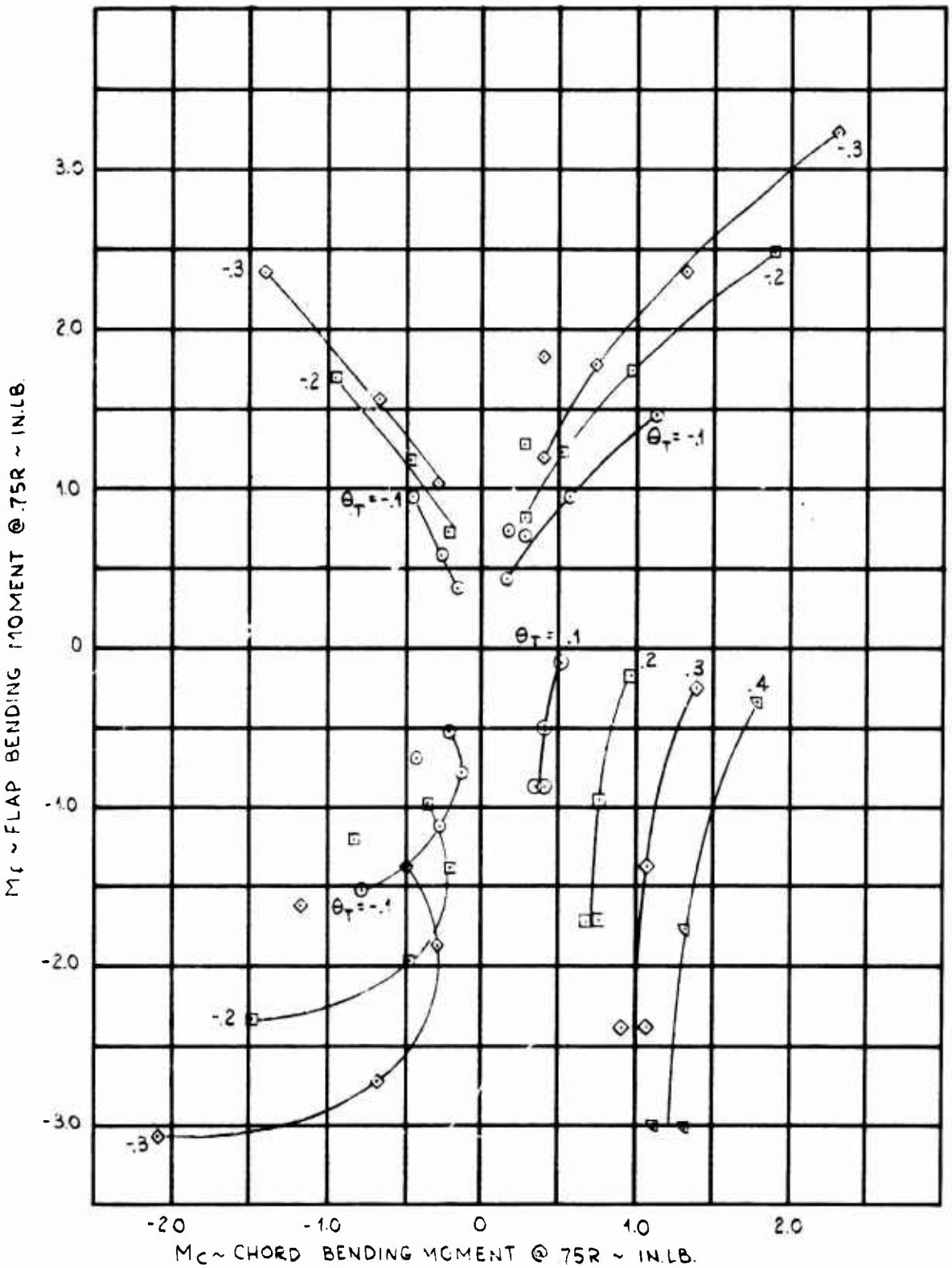

Figure 16. Blade No. 2 (Yellow) Deflection Data.

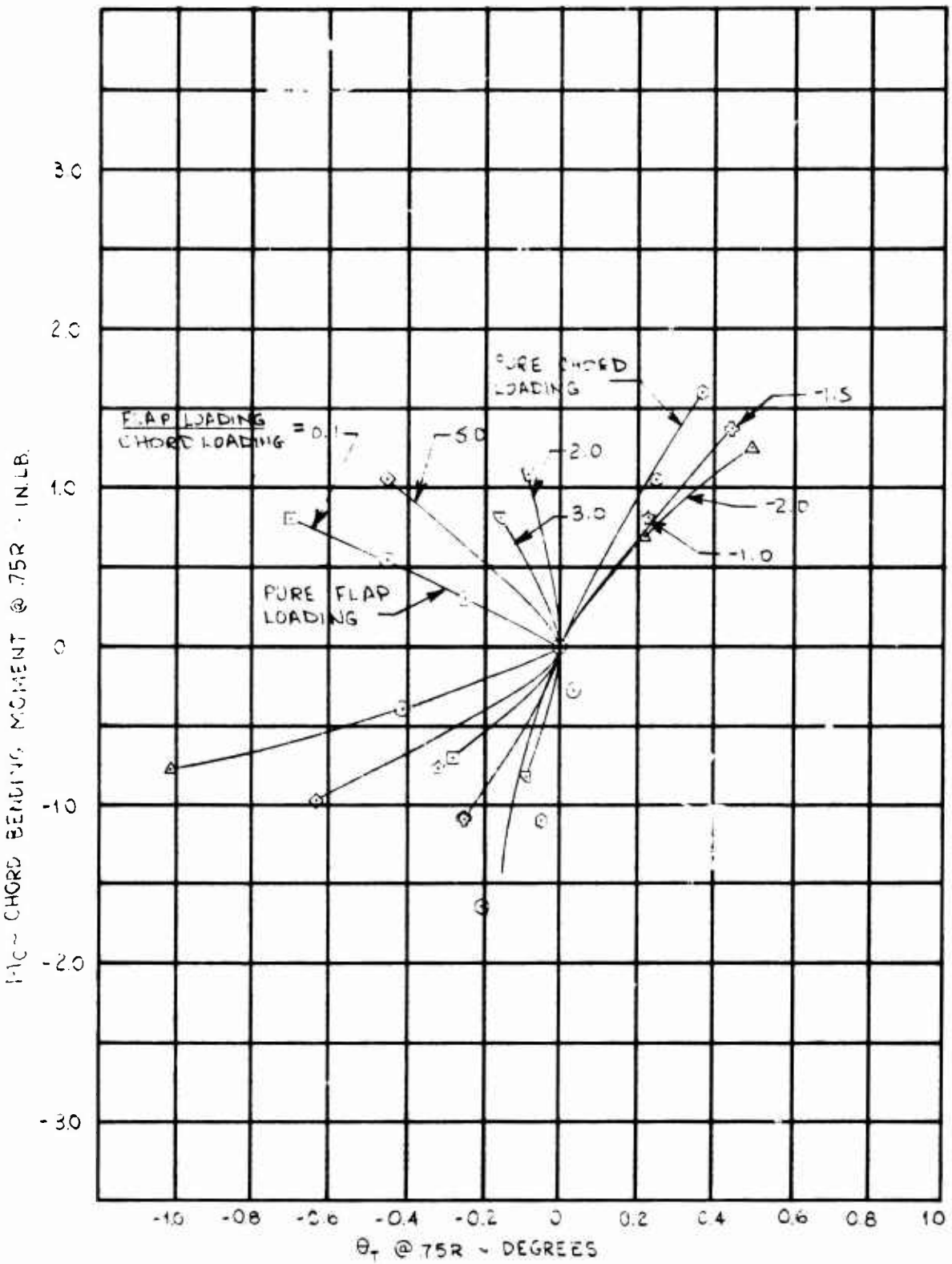

Figure 17. Blade No. 2 (Yellow) Deflection Data.

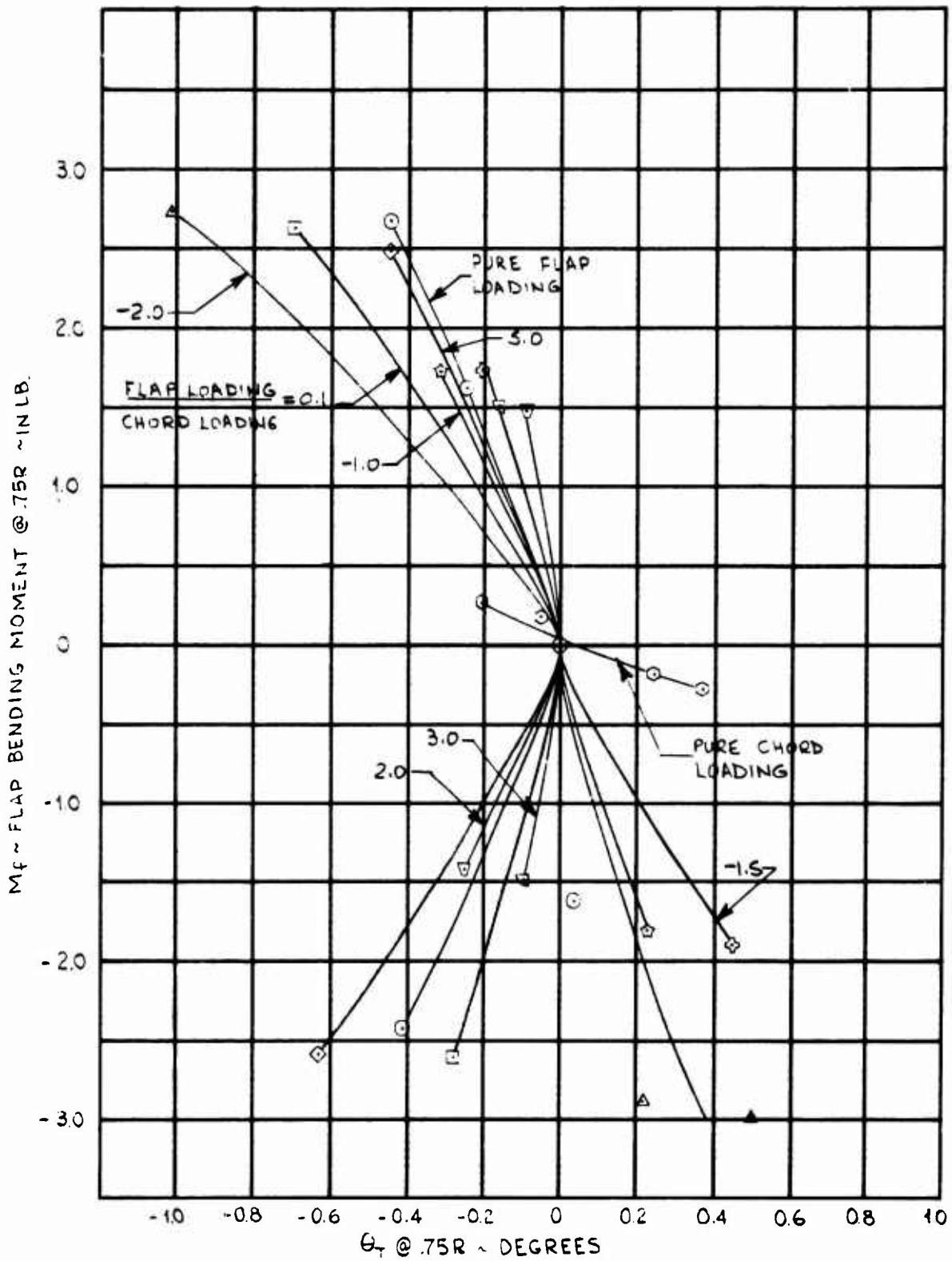

Figure 18. Blade No. 2 (Yellow) Deflection Data.

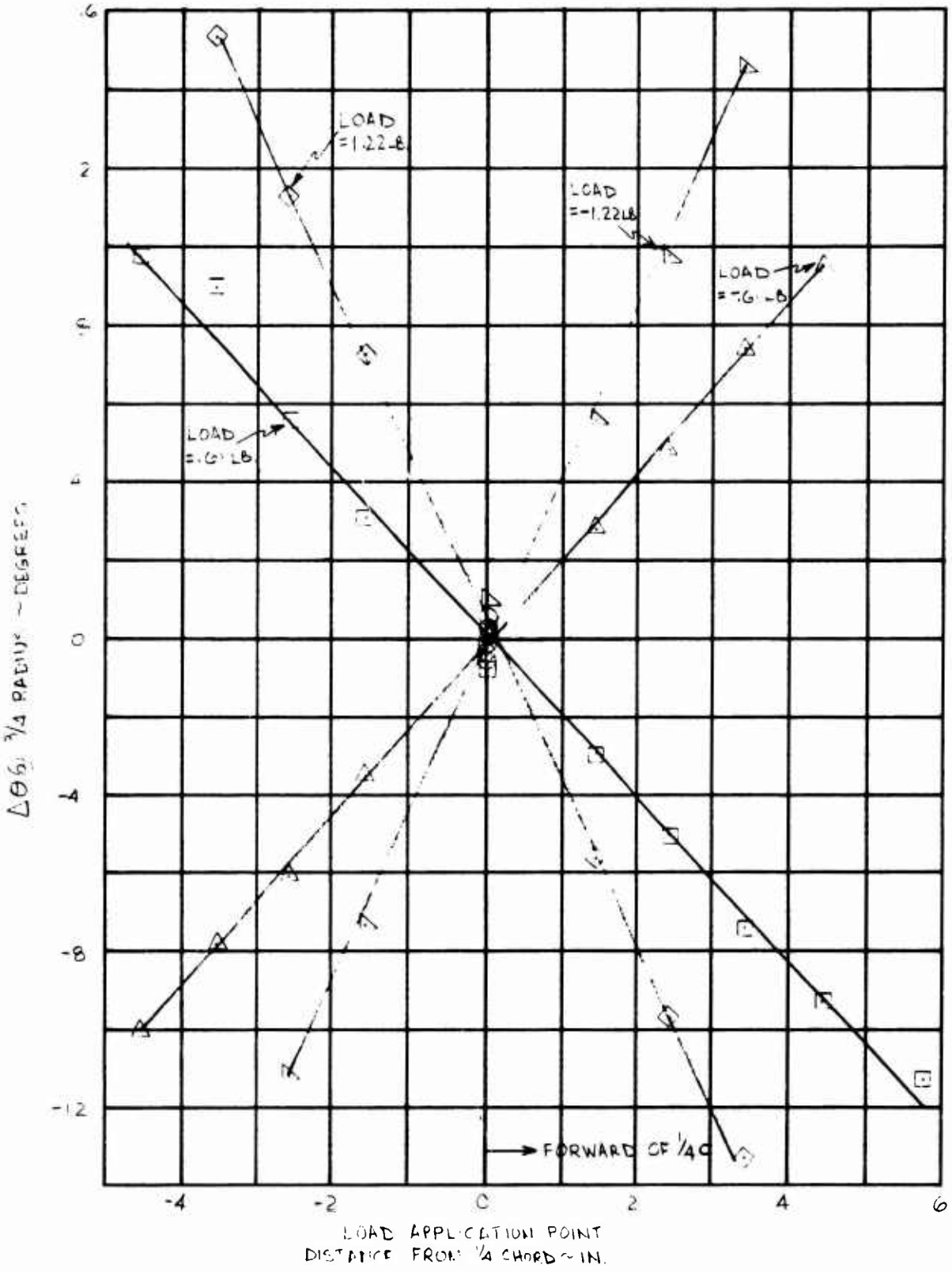

Figure 19. Blade No. 2 (Yellow) Shear Center Determination at 3/4 Radius.

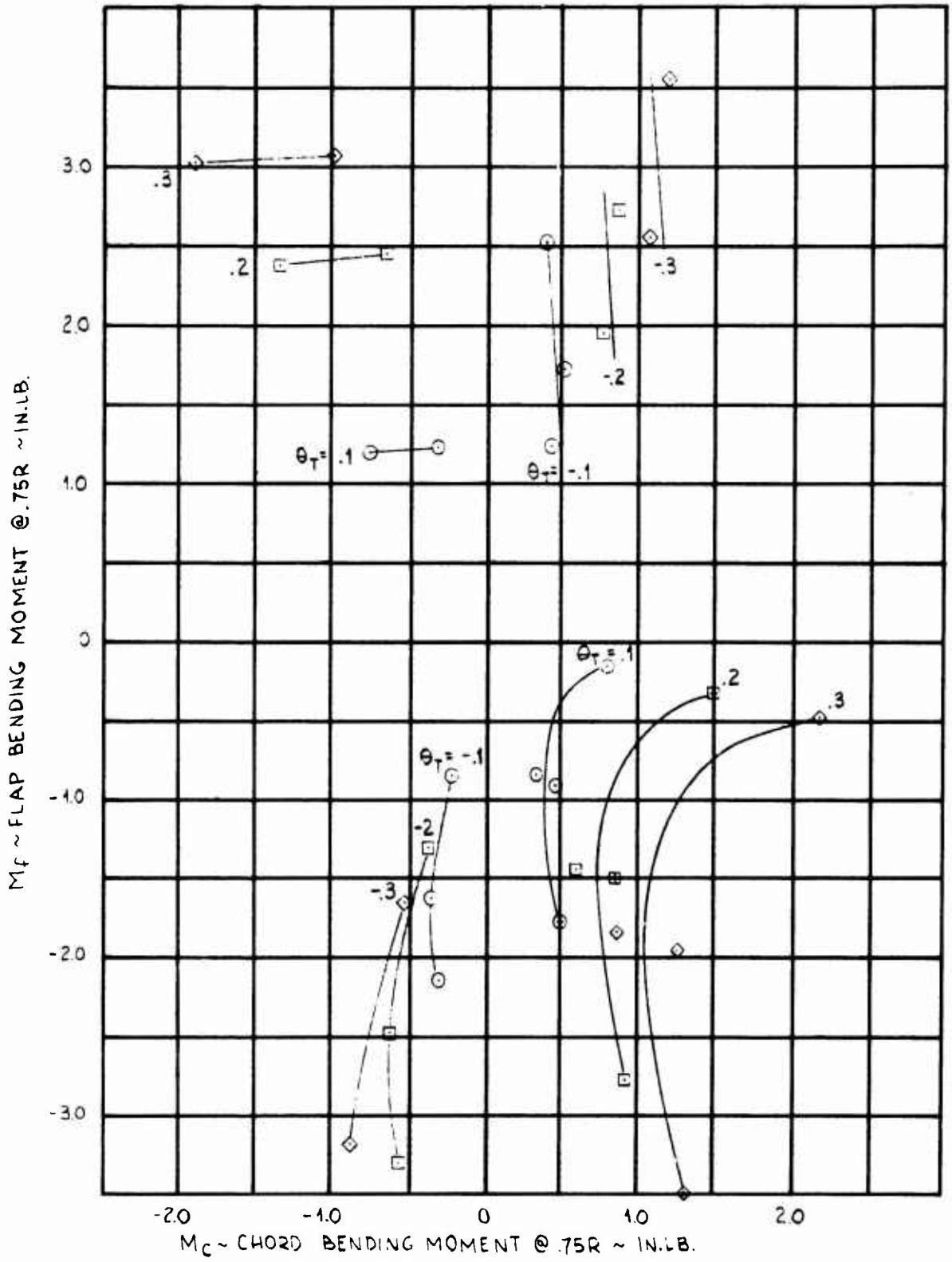

Figure 20. Blade No. 3 (Red) Deflection Data.

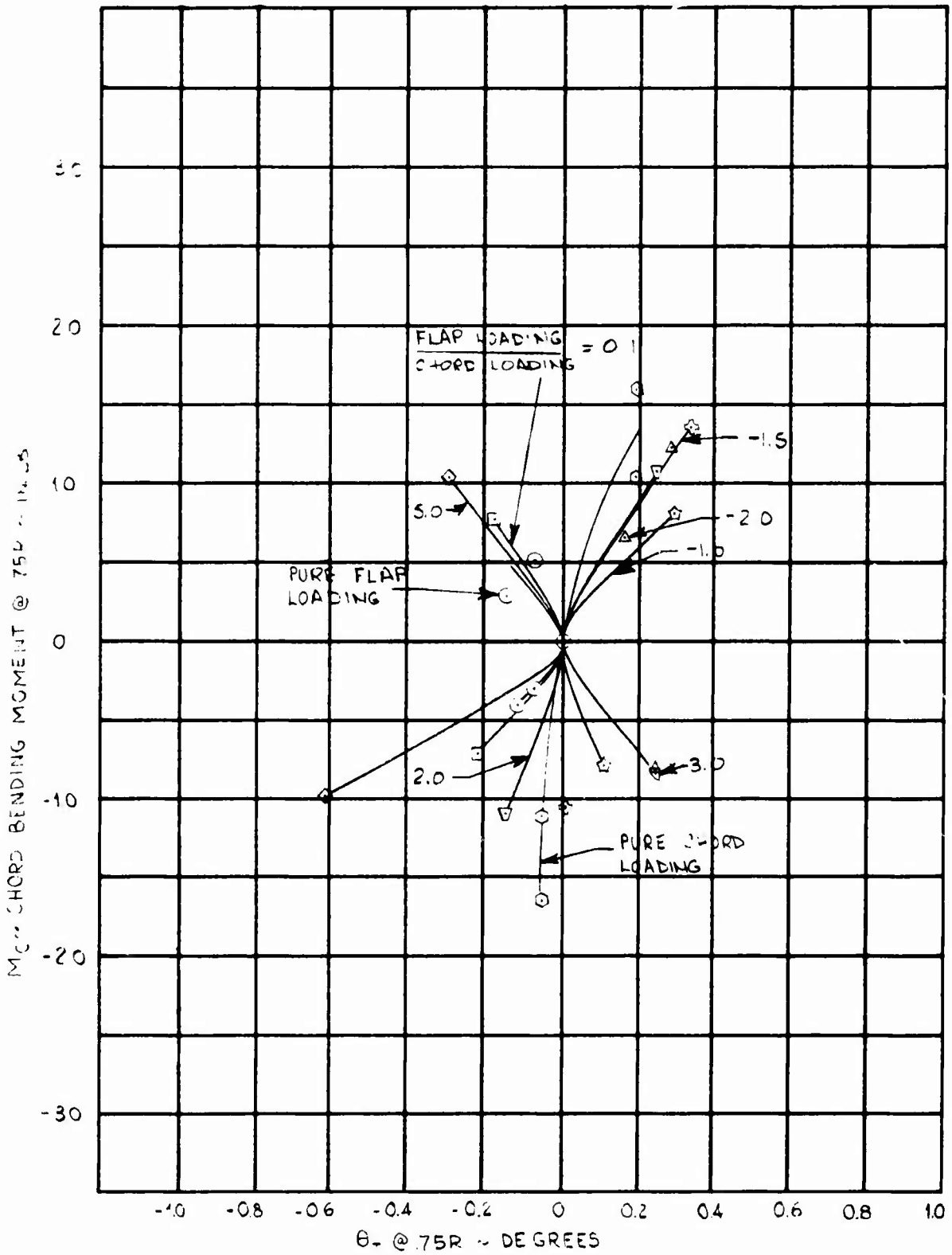

Figure 21. Blade No. 3 (Red) Deflection Data.

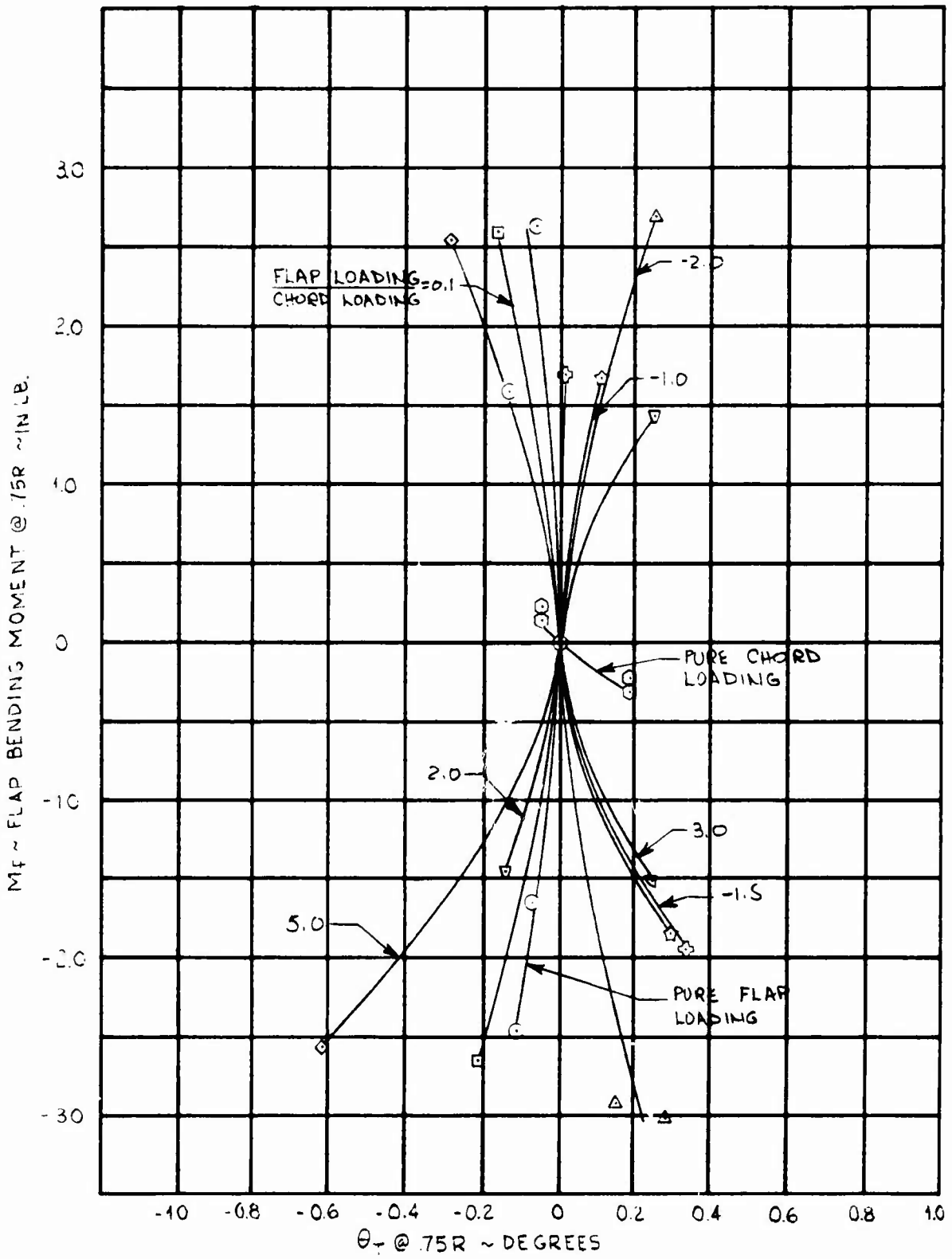

Figure 22. Blade No. 3 (Red) Deflection Data.

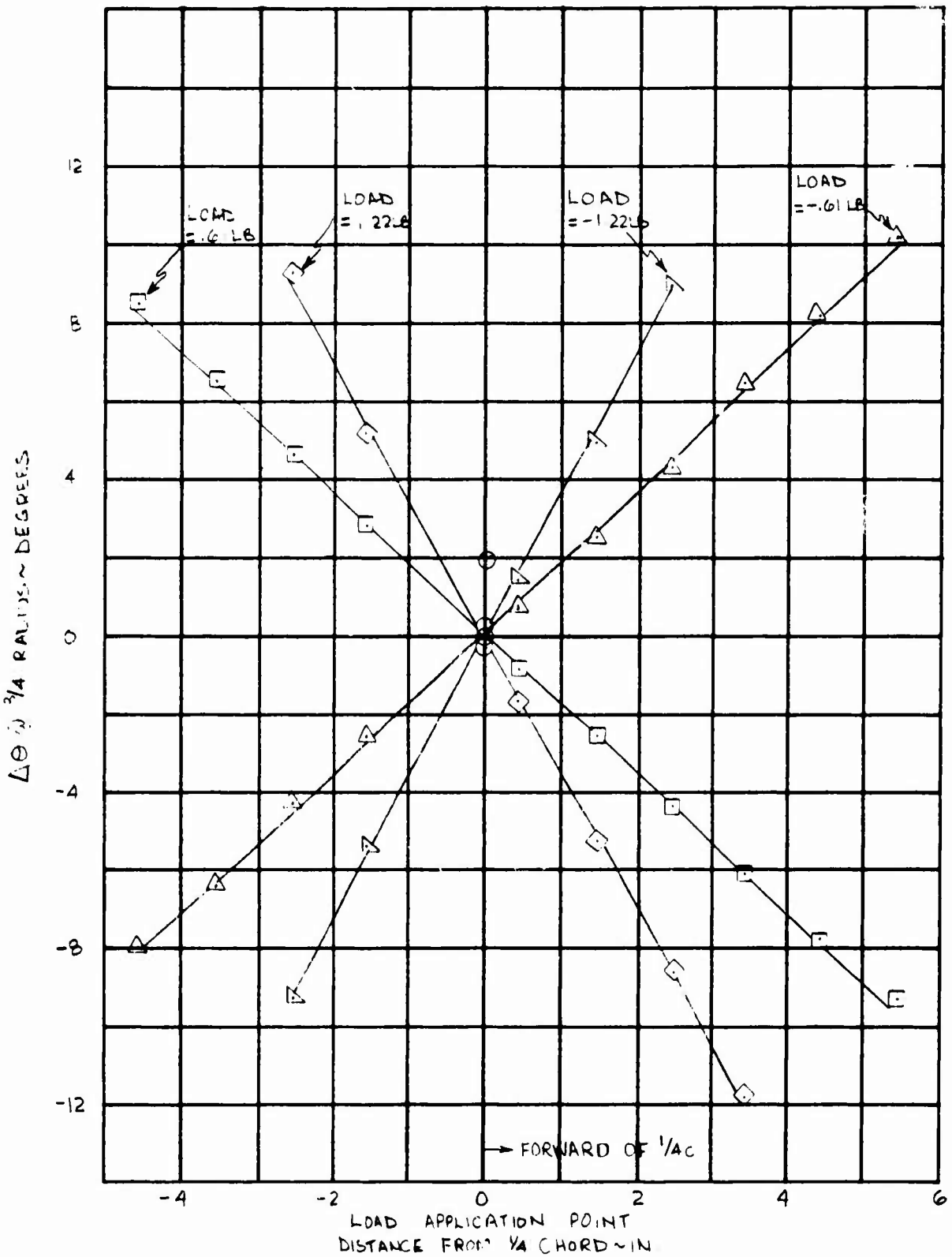

Figure 23. Blade No. 3 (Red) Shear Center Determination at 3/4 Radius.

TABLE XIII

BLADE DEFLECTION DATA - BLADE NO. 4 (GREEN)

[illegible]	[illegible]	[illegible]	[illegible]	[illegible]	[illegible]	[illegible]	[illegible]
	[illegible]	[illegible]	[illegible]	[illegible]	[illegible]	[illegible]	[illegible]
	.601	.131	.669	.582	-.12	816	-.294
	.382	.113	1.657	.324	-.24	.485	-.159
2	0	0	0	0	0	0	0
3	.365	-.057	-1.0[illegible]	-.[illegible]59	-.33	-.489	+.174
4	-.945	-.[illegible]81	-2.436	-.355	-1.[illegible]	.[illegible]33	.247
5	.[illegible]90	.159	2.6[illegible]8	.[illegible]89	-.[illegible]8[illegible]	+.778	-.238
6	.[illegible]30	248	[illegible]	.[illegible]01	-.93	.709	-.211
7	-.41	.131	[illegible]	.[illegible]249	-.40	.446	-.[illegible]32
8	.331	.249	1.4[illegible]9	1.165	.40	.426	-.065
9	-.045	.241	-.[illegible]71	1.[illegible]914	+.52	-.[illegible]54	.143
10	-.064	.364	-.[illegible]24	.[illegible]616	41	-.156	.212
11	-.404	.192	1.82	.[illegible]52	.28	-.586	.307
12	-.[illegible]41	.816	-1.9[illegible]	1.403	.82	-.6[illegible]1	.374
13	-.[illegible]65	.165	-2.[illegible]99	.732	.56	-.7[illegible]2	.40[illegible]
14	-.[illegible]72	.290	-2.[illegible]	1.2[illegible]57	.14	-.957	457
15	.[illegible]04	-.046	2.[illegible]1	-.204	-.12	.[illegible]15	-.549
16	.601	-.169	2.[illegible]4	-.[illegible]75[illegible]	+.25	.[illegible]80[illegible]	-.368
17	.[illegible]20	-.168	1.[illegible]3[illegible]	-.746	.15	.[illegible]52[illegible]	-.259
18	.384	-.227	1.[illegible]05	-1.00[illegible]	.18	.530	-.293
19	.[illegible]29	-.43	.[illegible]15	-1.079	.06	.[illegible]84[illegible]	-.129
20	.56	-.365	.249	-1.620	-.83	.[illegible]30	-.159
21	-.[illegible]22[illegible]	-.[illegible]175	-1.[illegible]47[illegible]	-.[illegible]195	-.40	-.426	+.109
22	-.319	-.240	-1.416	-1.06[illegible]8	-.61	-.391	.068
23	-.[illegible]539	-.[illegible]149	-2.[illegible]15	-.661	-.89	-.775	.[illegible]28

TABLE XIV

BLADE DEFLECTION DATA - BLADE NO. 1 (BLUE)

STATION	APPLIED LOADS - LB.		MOMENTS @ ... - IN.-LB.		DEFLECTIONS @ ... IN.		
	FLAP	CHORD	FLAP	CHORD	ANGULAR	FLAP - IN.	CHORD - IN.
1	.601	.131	2.668	.582	-.43	.840	-.255
2	.362	.073	1.607	.324	-.52	.398	-.158
3	0	0	0	0	0	0	0
4	-.265	-.057	-1.620	-.253	-.10	-.500	+.168
5	-.548	-.031	-2.433	-.360	-.31	-.763	.239
6	.590	.189	2.619	.839	-.87	+.796	-.233
7	.580	.245	2.5[illegible]	1.088	-.86	.779	-.180
8	.341	.190	1.514	.843	-.84	.550	-.096
9	.331	.249	1.469	1.105	-.49	.427	-.067
10	-.043	.242	-.191	1.074	+.24	-.101	.127
11	-.064	.364	-.284	1.616	.39	-.152	.191
12	-.409	.191	-1.816	.848	.54	-.603	.287
13	-.430	.314	-1.909	1.394	78	-.658	.347
14	-.653	.163	-2.899	724	.29	-.937	.386
15	-.675	.288	-2.996	1.278	1.00	-.982	.428
16	.604	-.049	2.681	-.218	-.08	+.830	-.327
17	.605	-.171	2.686	-.759	-.42	.845	-.347
18	.379	-.168	1.682	-.746	-.01	.554	-.251
19	.382	-.228	1.696	-1.012	-.24	.561	-.277
20	.039	-.243	.173	-1.079	-.22	.096	-.119
21	.056	-.365	.249	-1.620	-.18	.127	-.167
22	-.333	-.179	-1.478	-.795	-.24	-.438	+.099
23	-.318	-.240	-1.412	-1.065	-.26	-.423	.063
24	-.588	-.148	-2.610	-.657	-.51	-.796	.234
25	-.569	-.212	-2.526	-.941	-.09	-.730	.181

TABLE XV

BLADE DEFLECTION DATA - BLADE NO. 2 (YELLOW)

CASE	APPLIED LOAD @ TIP LE		MOMENTS @ TIP LE		DEFLECTION @ .75 L		
	FLAP	CHORD	FLAP	CHORD	ANGULAR θ-DEG	FLAP AT .75 IN.	CHORD AT .75 IN.
1	.601	.126	2.668	.559	-.46	.622	-.206
2	.362	.071	1.607	.315	-.26	.381	-.119
3	0	0	0	0	0	0	0
4	-.365	-.058	-1.620	-.257	+.03	-.372	.136
5	-.547	-.084	-2.428	-.373	-.42	-.571	.193
6	.591	.184	2.623	.817	-.71	+.638	-.178
7	.581	.242	2.579	1.074	-.46	.614	-.144
8	.341	.189	1.514	.839	-.17	.354	-.065
9	.331	.247	1.469	1.096	-.10	.337	-.029
10	-.043	.242	-.191	1.074	+.24	-.085	+.138
11	-.064	.364	-.284	1.616	.36	-.119	.200
12	-.408	.190	-1.811	.843	.22	-.472	.267
13	-.430	.313	-1.909	1.389	.44	-.603	.323
14	-.652	.160	-2.894	.710	.21	-.728	.343
15	-.674	.286	-2.992	1.270	.49	-.771	.410
16	.609	-.051	2.703	-.226	-.44	+.682	-.292
17	.615	-.171	2.730	-.759	-1.03	.666	-.335
18	.384	-.168	1.705	-.746	-.33	.436	-.238
19	.390	-.228	1.731	-1.012	-.21	.439	-.265
20	.040	-.243	.178	-1.079	-.06	.069	-.125
21	.057	-.365	.253	-1.620	-.21	.103	-.181
22	-.335	-.181	-1.487	-.803	-.10	-.345	+.066
23	-.321	-.242	-1.425	-1.074	-.26	-.312	.044
24	-.590	-.153	-2.619	-.679	-.29	-.617	.183

TABLE XVI

BLADE DEFLECTION DATA - BLADE NO. 3 (RED)

CASE	APPLIED LOADS @ .75R-LB		MOMENTS @ .75R-IN-LB		DEFLECTIONS @ .75R		
	FLAP	CHORD	FLAP	TORQUE	INCIDENCE-DEG	FLAP-IN	CHORD-IN
1	.602	.122	2.672	.542	-.08	.666	-.158
2	.363	.069	1.611	.306	-.15	.323	-.089
3	0	0	0	0	0	0	0
4	-.364	-.060	-1.616	-.266	[illegible]	-.412	+.108
5	-.547	-.086	-2.428	-.382	.12	-.619	+.158
6	.592	.180	2.628	.799	-.18	.662	-.140
7	.581	.239	2.579	1.061	-.31	.647	-.117
8	.342	.188	1.518	.835	-.15	.390	-.050
9	.331	.247	1.469	1.096	.24	.387	-.034
10	-.043	.242	-.191	1.074	.18	-.064	+.111
11	-.064	.364	-.284	1.616	.18	-.110	.154
12	-.108	.188	-1.811	.835	.29	-.472	.218
13	-.430	.311	-1.909	1.381	.53	-.485	.269
14	-.651	.156	-2.890	.692	.15	-.725	.277
15	-.673	.281	-2.987	1.247	.28	-.753	.329
16	.611	-.057	2.712	-.253	-.28	+.665	-.224
17	.616	-.178	2.734	-.790	+.24	681	-.262
18	.384	-.171	1.705	-.759	10	.450	-.189
19	.389	-.230	1.727	-1.021	0	.455	-.217
20	.040	-.243	.178	-1.079	-.06	.065	-.102
21	.0581	-.365	257	-1.620	-.06	.091	-.158
22	-.334	-.182	-1483	-.808	+.24	-.360	.056
23	-.320	-.242	-1.420	-1.074	-.15	-.337	034
24	-.589	-.155	-2.615	-.688	-.22	-.636	.144
25	-.571	-.217	-2.535	-.963	-.62	-.622	.117

SECTION IV

MODEL AND WIND TUNNEL DETAILS

1. MODEL DESCRIPTION

1.1 GENERAL

The model tested consisted of a left wing/nacelle assembly and a 3-bladed unpowered rotor. The model blades were of the hingeless, soft in-plane type and were dynamically representative of a typical folding tilt-rotor design. The rotor diameter was 33.75 inches and the rotor solidity was 0.102. Figure 24 illustrates the general arrangement of the model and Figure 25 shows the model mounted in the test section of the Princeton University wind tunnel. Model dimensions are given in Table XVII.

1.1.1 Wing/Nacelle Details

The model wing had an NACA 63A415.5 section and a 0.3 chord, single-slotted, full-span flap, manually adjustable over a ±30-degree range. The wing was geometrically scaled only and the nacelle was oversized (compared to a typical full-scale design) in order to accommodate sliprings, instrumentation, and the collective pitch actuating system. Details of the nacelle structure are shown in Figure 26.

The wing was not dynamically scaled but was sufficiently flexible that the mounting frequencies coupled with the rotor. The dynamic data relating to these modes were not directly scalable; however, they provide some valuable guidelines for full-scale design.

The wing airfoil was removable, as illustrated in Figure 27, to allow isolation of the effect of the wing aerodynamics on the rotors.

The model mounting baseplate, wing spar, and nacelle box structure were fabricated of aluminum alloy and bolted together. The wing and flap contours were shaped of wood and fixed to the wing spar; the nacelle contours were formed of a polyester resin on a wooden base which in turn was laminated to a thin-wall, aluminum-alloy cylinder. The inside surface of this cylinder was positioned and secured to bulkheads attached to

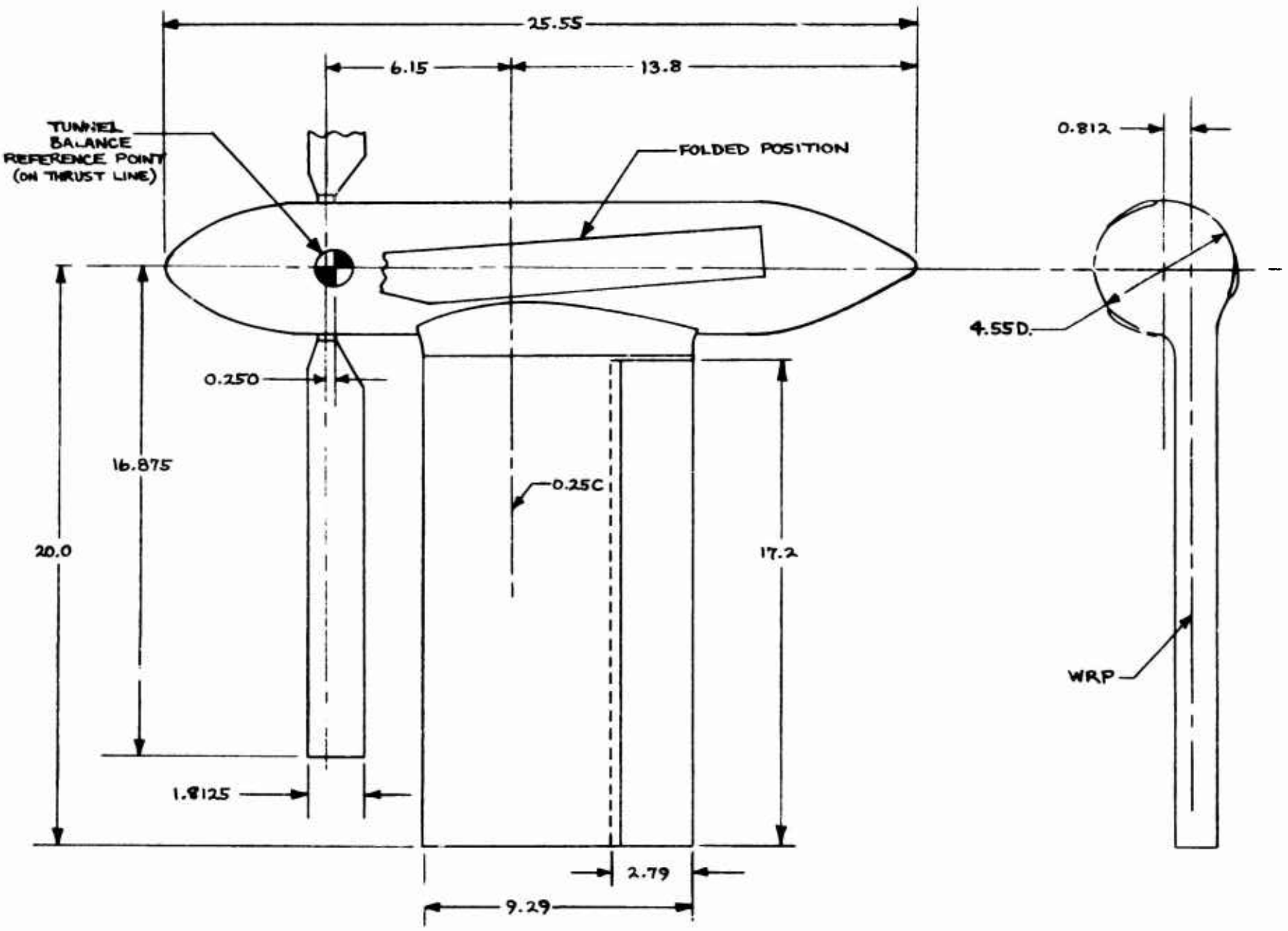

Figure 24. Semispan Folding Tilt-Rotor Model Test Setup.

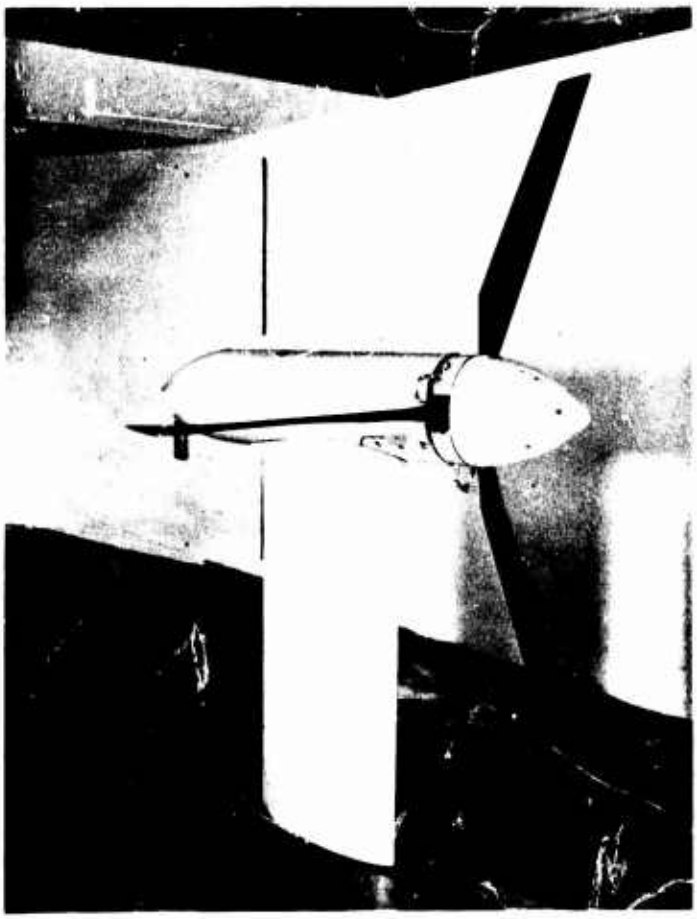

Figure 25. Model 213, 1/16-Scale Semispan Conversion Model Installed in Princeton University Low-Speed Wind Tunnel.

TABLE XVII

MODEL DIMENSIONS

ROTOR

Number of Blades	3
Disc Area	894.62 in^2
Solidity	0.102
Blade Radius	16.875 in
Blade Chord (Non-Tapered)	1.813 in
Blade Airfoil Sections	230XX

Blade Characteristics

r/R	Twist, Deg.	Thickness, t/c
.2	24.2	.250
.3	20.75	.143
.4	17.3	.127
.5	13.8	.120
.6	10.35	.115
.7	6.9	.109
.8	3.45	.103
.9	0	.097
1.0	-3.45	.090

WING

Airfoil	NACA 63A415.5
Span (℄ Nacelle to Tunnel Floor)	20.0 in
Chord (Constant)	9.29 in
Area	185.8 in^2
Aspect Ratio	2.15
Flap	0.3 Chord, Single-Slotted

NACELLE (Not Scaled)

Overall Length	25.55 in
Maximum Diameter	4.55 in
Angle of Incidence (W.R.T. Wing)	0.0°

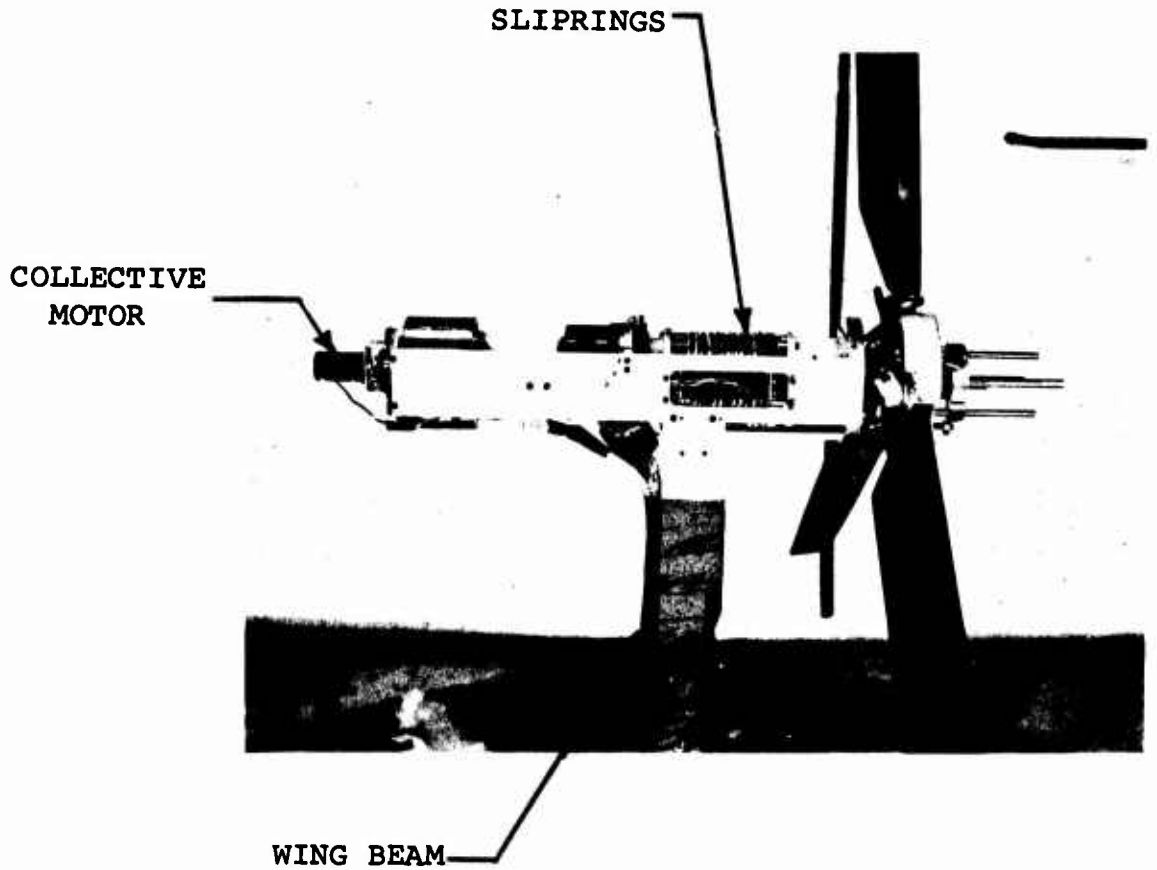

Figure 26. Model 213, 1/16-Scale Semispan Conversion Model, Details of Rotor Hub and Nacelle Contents.

Figure 27. Model 213, 1/16-Scale Semispan Conversion Model With Wing Airfoil Removed.

the nacelle box structure. A hollow wooden tail cone was used as the aft end of the nacelle and was readily removable for access to the feathering mechanism. The entire nacelle fairing was removable for complete access to the internal mechanisms and instrumentation.

Prior to the test program, the stiffnesses of the model wing and support structure were measured giving the following results:

Chordwise	1,130 lb/in.
Lift	800 lb/in.
Torsion	65,000 in.-lb/radian

The deflections are rotor hub deflections or angular motions of the rotor shaft, respectively. To further define the aeroelastic/dynamic properties of the wing, tests were performed to measure the natural frequencies of the wing with the nonrotating rotor. These tests were performed at various times during the test program. The results presented in Table XVIII show the effects of changes made to the wing during testing. Testing prior to run 84 with the wing airfoil removed shows lower-than-expected frequencies. Wires were added to the model prior to run 95 to increase the wing chordwise stiffness.

1.1.2 Blade Details

The model blades had a radius of 16.875 inches, a constant chord of 1.81 inches, and were twisted 30.25 degrees from the center of rotation to the tip. Their structure was composed of one layer of 0.003-inch glass-fiber cloth laminated to a urethane foam core with epoxy resin. The foam core was bonded to the blade spar which consisted of 0.500-inch by 0.03125-inch precision flat-ground stock, twisted to conform to the blade twist and riveted and soft-soldered to the blade root fitting. A plan view of the blade is shown in Figure 28, together with the blade twist distribution and the locations of the strain gages used to measure blade bending. Figure 29 is a detailed view of the blade root fitting. Blade inspection results for the four blades manufactured for this test are given in Figure 30. In general, the blades conformed well to the specified twist and chord length but were thicker than specified.

TABLE XVIII

WING NATURAL FREQUENCY TEST HISTORY

TEST WAS PERFORMED BEFORE RUN	MODEL CONFIGURATION	NATURAL FREQUENCIES, CPS		
		CHORDWISE	FLAPWISE	TORSION
23	Airfoil On	31.6	24.0	42.8
Repeat	Airfoil On	30.0	24.0	42.8
84	Airfoil Off	26.7	22.2	41.1
85	Airfoil Off	30.0	23.1	37.9
95	Airfoil Off (Stiffened)	33.3	-	41.1
Repeat	Airfoil Off	35.1	-	..
Repeat	Airfoil Off	33.3	-	-

NOTES: Model installed in tunnel with rotor not rotating.

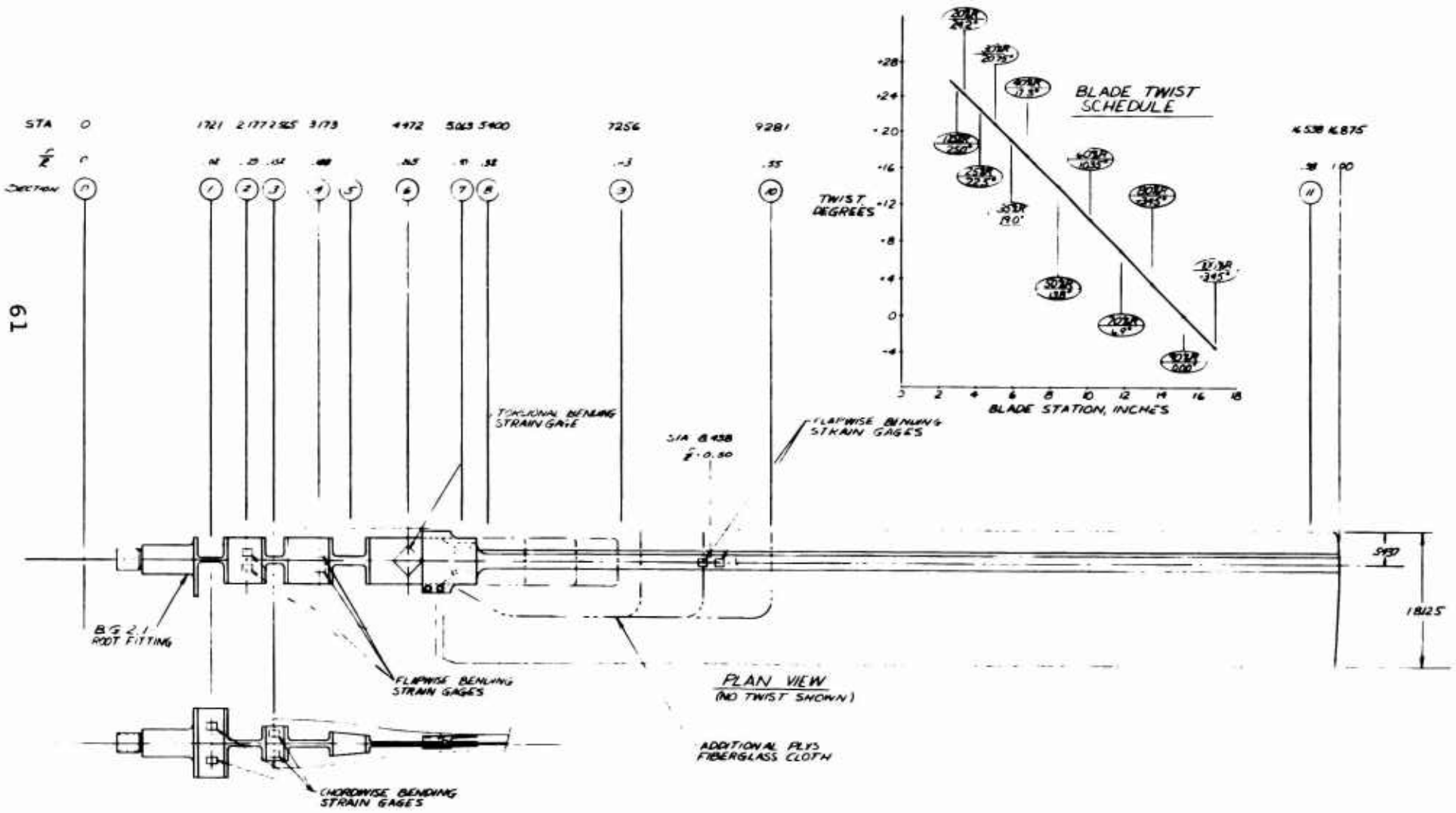

Figure 28. Plan View of Blade Showing Twist and Instrumentation Locations

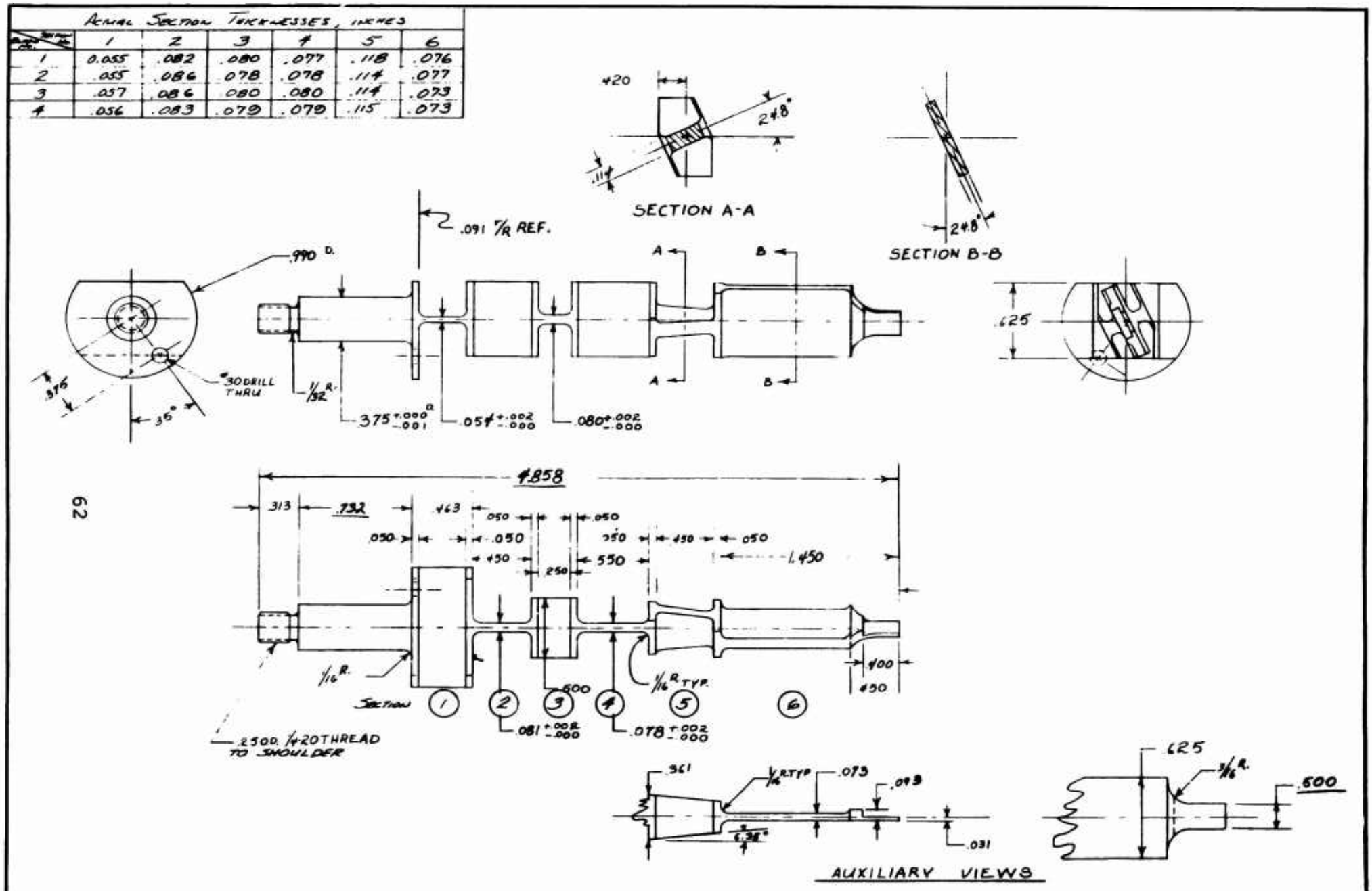

62

Figure 29. Blade Root End Fitting.

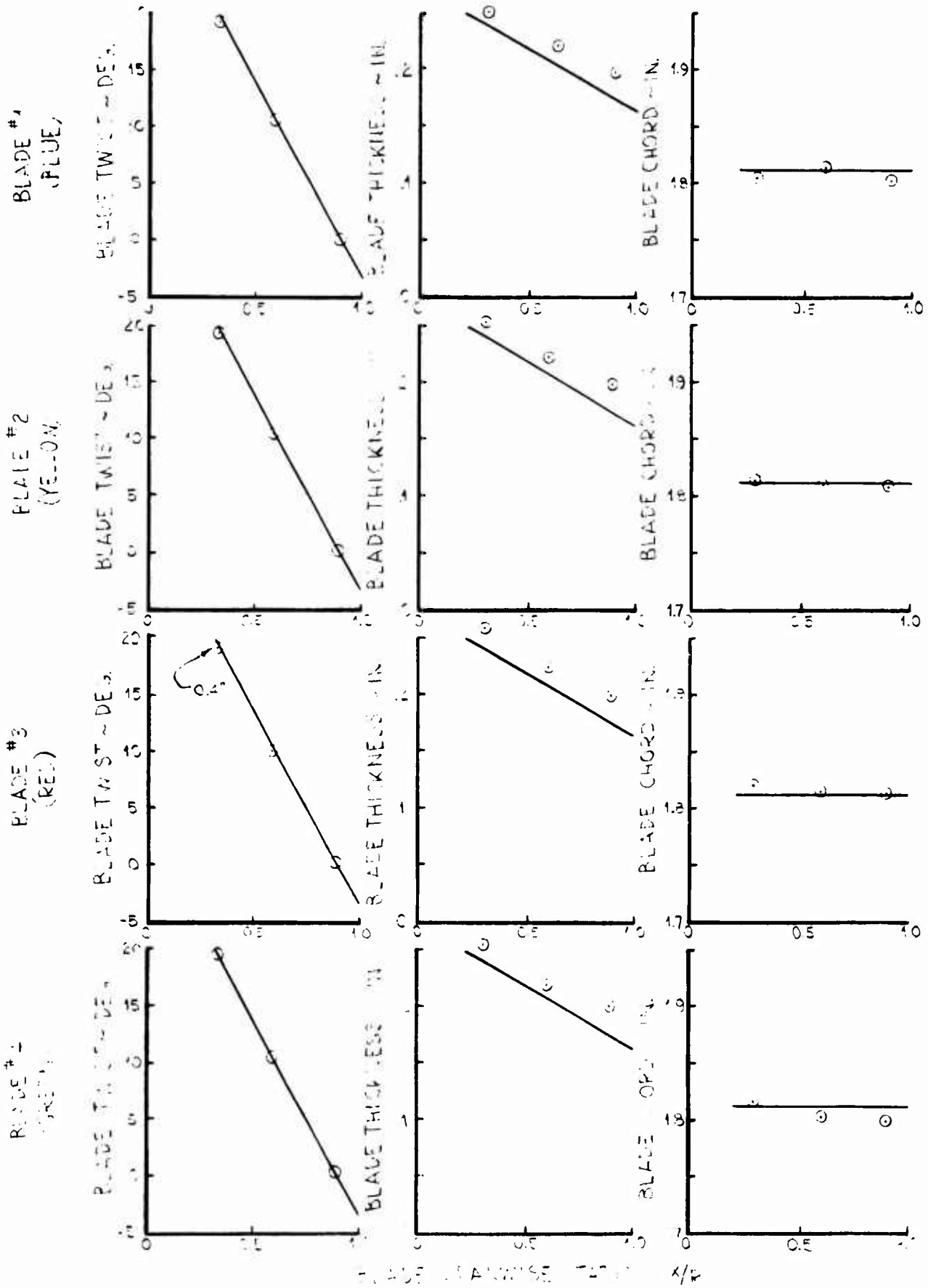

Figure 30. Blade Geometry Inspection Data.

The model blades were designed to conform as closely as practicable to full-scale dynamic properties. Due mostly to outboard instrumentation and the desire to avoid structural discontinuities in the interest of structural integrity, exactly scaled elastic and mass distributions could not be obtained. However, the criterion of having a rotating flapwise natural frequency/rotational speed = 1.4 at 2,000 rpm was satisfied. Blade inertial and elastic properties are presented in Table XIX. The calculated model flapwise and chordwise natural frequencies at zero rpm, 16 cps, and 25.5 cps, respectively, correlated well with model frequencies measured by blade static disturbance (tweak) tests conducted throughout the program. A history of these tweak test results is shown in Figures 31 and 32 for the two instrumented blades tested. The rate of decay of the oscillation that resulted from the static disturbance was also measured and is presented in these figures. These data show an initial reduction in the blade natural frequencies of about 10 percent when the blades were mounted on the model, as compared to the rigid mounting of the bench test. This caused the flapwise frequency to be less than the design value. A blade root end reinforcement fix was added to the blades after run 22 and this increased the flapwise frequency to the design values. The damping data shown are of the magnitude expected from structural damping. Measured rotating blade frequencies are given in Part I.

1.2 INSTRUMENTATION

1.2.1 Blade Instrumentation

Two of the three rotor blades used in the test program were instrumented to measure torsion, chordwise bending, and flapwise bending at the stations indicated in Figure 28; the third and spare blades were uninstrumented. Table XX lists the specific measurements taken during the test, their posisions on the recording equipment, calibration constants, and the symbols used to denote each gage in the data.

The blade instrumentation consisted of full bridges of 120-ohm constant foil strain gages excited in parallel by a 5.0-volt d.c. $\pm$0.1-percent regulated power supply. Strain-gage power and output signals were transferred from the rotating to the stationary system by means of a 24-ring pancake-type slipring assembly.

TABLE XIX

BLADE INERTIAL AND ELASTIC PROPERTIES

RADIAL STATION r/R	FLAPWISE STIFFNESS EI_{FLAP} (LB-IN^2)	CHORDWISE STIFFNESS EI_{CHORD} (LB-IN^2)	TORSIONAL STIFFNESS GJ (LB-IN^2)	WEIGHT W (LB/IN)
.091 - .113	128×10^3	270	48×10^3	.0136
.116 - .142	780	45×10^3	17×10^3	.0142
.145 - .160	21×10^3	720	7.9 x 10	.0119
.163 - .195	690	43×10^3	16×10^3	.0136
.198 - .225	13 - 4.4×10^3	1370 - 1040	4.9×10^3 - 1.7×10^3	.0122 - .0085
.228 - .287	640	41×10^3	15×10^3	.0133
.287 - .330	4300	17.9×10^3	7.5×10^3	.0114
.340	1580	7.8×10^3	3.54×10^3	.0071
.430	390	6.75×10^3	2.77×10^3	.0053
.550	188	5.62×10^3	2.26×10^3	.0052
.980	137	5.63×10^3	2240	.0051

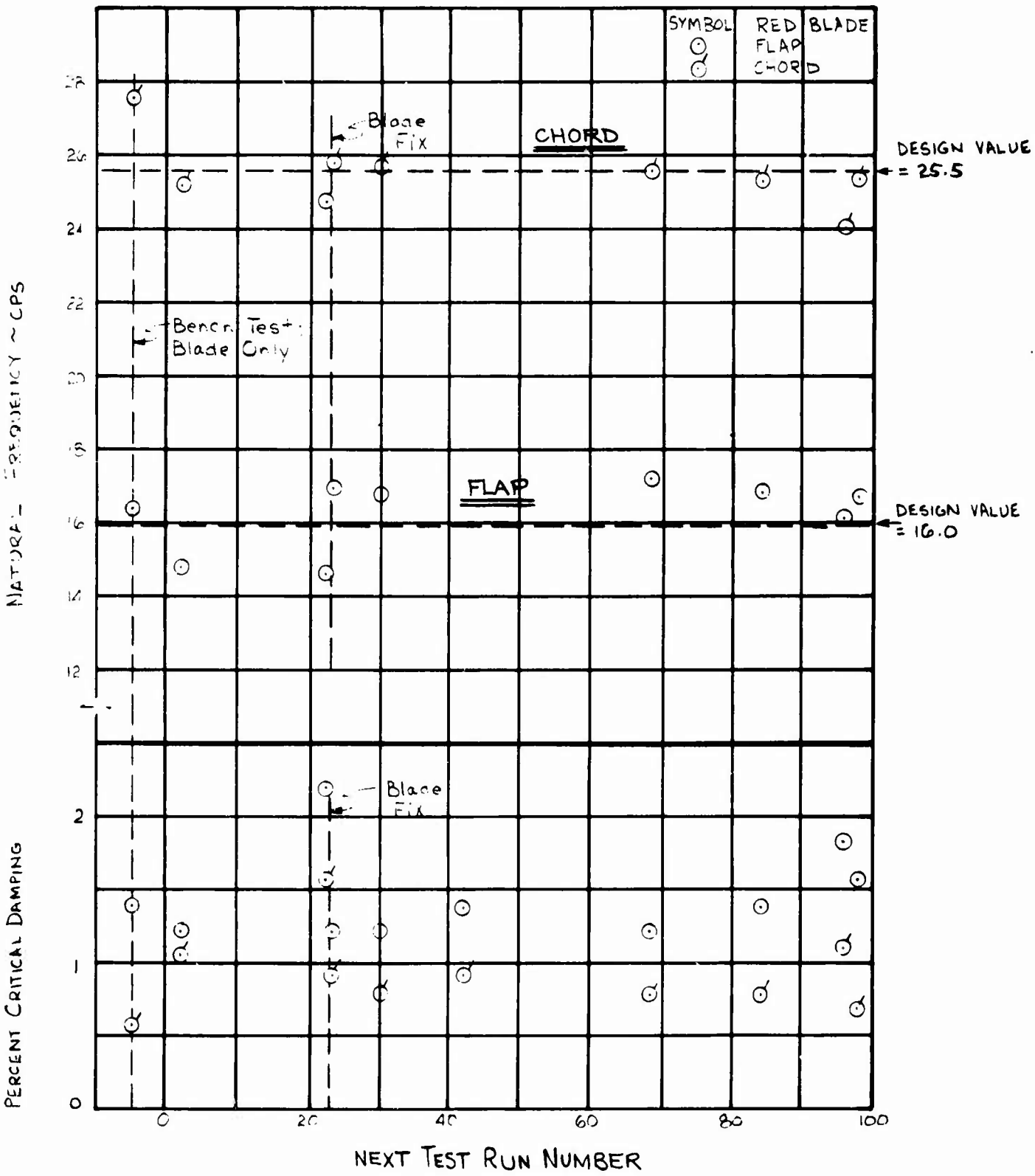

Figure 31. Blade Natural Frequencies and Damping From Static Disturbance Tests of Red Blade.

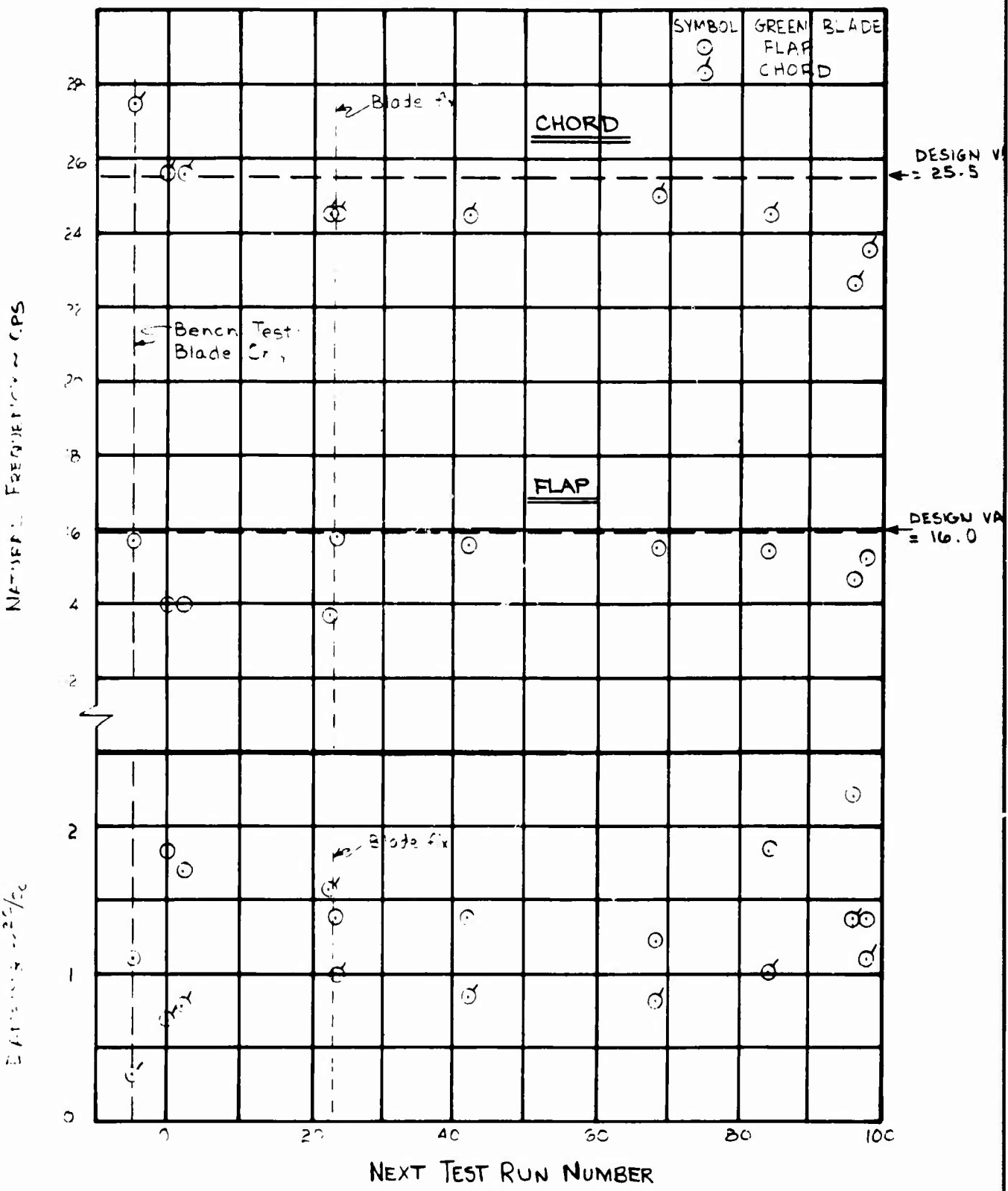

Figure 32. Blade Natural Frequencies and Damping From Static Disturbance Tests of Green Blade.

TABLE XX

INSTRUMENTATION AND CALIBRATIONS USED IN TEST

GAGE	SYMBOL	BLADE	CHANNEL	RECORDER	RUNS	R_{CAL} EQUIV. (IN-LB)	K_{FACTOR} (N-LB/IN.)	FREQ. RESPONSE (CPS)
FLAP @ .13R	⊙	RED	1	HONEY	-22	8.012	7.35	90
"	"	"	"	"	23-97		14.70	"
FLAP @ .5R	⊙	GREEN	6	CEC	30-97	2.75	8.6	90
CHORD @ .2R	◇	RED	3	HONEY	1-22	6.660	12.11	90
"	"	"	"	"	23-97		30.3	"
CHORD @ .2R	⊙	GREEN	10	CEC	1-22	7.59	9.06	90
"	"	"	"	"	23-97		22.6	"
CHORD @ .11R	▽	RED	2	HONEY	1-22	8.380	13.97	90
"	"	"	"	"	23-97		28.0	"
TORSION @ .2R	⊡	GREEN	11	CEC	1-29	3.77	3.66	90
TORSION @ .2R	◇	RED	4	HONEY	1-97	3.830	3.39	90
WING DRAG	D	GREEN	3	CEC	1-47		9.0	90
" "	"	"	"		48-55		14.2	≈45
" "	"	"			56-59		7.0	"
" "	"	"			60		"	30
" "	"	"		"	61-68		9.0	90
" "	"	"	"		69		7.0	30
" "	"	"	"		70-97		9.0	90
WING PITCHING MOMENT	◺	GREEN	5	CEC	1-47		100.0	90
" "	"	"		"	48-55		160.0	"
" "		"	"		56-59		"	"
" "	"	"	"		60		"	"
" "	"	"	"	"	61-68		100 0	"
" "	"	"	"	"	69		160.0	"
" "	"	"	"	"	70-97		100.0	"
WING LIFT	A	GREEN	7	CEC	1-47		22.0	90
" "			"		48-55		35.0	"
" "	"	"	"		56-59		"	"
" "	"	"	"	"	60		"	"
" "	"	"	"		61-68		22.0	"
" "	"	"		"	69		35.0	"
" "	"	"			70-97		22.0	"
ROTOR RPM	◈		14	CEC	1-97			90
" "	"		7	HONEY	1-97			"
COLLECTIVE PITCH	θ		13	CEC	1-97		23.65°/IN.	90
" "	"		9	HONEY	1-97		47.67°/IN.	"

1.2.2 Wing Mount Force-Measuring System

The complete wing-nacelle-rotor system was mounted on a 3-component strain-gage balance system designed to measure the transient lift, drag, and pitching moment of the model as a function of rotor speed and acceleration. The system consisted of two parallel plates connected by flexural supports. The lower plate was secured to the tunnel floor and the upper plate was restrained from in-plane translation by means of two orthogonal strain gages measuring body axis lift and drag forces. Rotation in the plane was resisted by a third gage which measured pitching moment.

1.2.3 Nacelle Instrumentation

The model nacelle contained instrumentation to measure blade collective pitch, blade azimuth position, and angular velocity. The blade pitch control system followup potentiometer was also used as the collective pitch data instrument. Rotor azimuth position was measured by means of a precision conducting plastic single-turn potentiometer geared down from the rotor shaft so as to rotate one revolution for every two revolutions of the rotor. Rotor angular velocity was measured by a d.c. tachometer also geared to the rotor shaft.

1.2.4 Conditioning and Recording Equipment

All of the model blade and balance strain-gage signals were processed by either d.c. or carrier amplifier equipment supplied as part of the wind tunnel instrumentation system. Four channels of blade strain-gage data from blade No. 3 (red blade) plus rotor rpm and collective pitch were recorded on a Honeywell Visicorder direct-writing oscillograph. The three model balance strain-gage channels plus three channels of blade strain-gage data from No. 4 (green blade) and rotor rpm and collective pitch were recorded on a CEC direct-writing oscillograph; types and serial numbers of this equipment are listed in Table XY.I. During windmilling test runs, rotor rpm was read on-line by means of a digital voltmeter display.

1.3 BLADE PITCH CONTROL SYSTEM

1.3.1 Electronic System

The blade pitch control system was a high-gain, proportional-feedback control system. Its function was to position the

TABLE XXI

RECORDING EQUIPMENT UTILIZED FOR GREEN BLADE DATA

DESCRIPTION	TYPE	SERIAL NUMBERS
Oscillator Power Supply	2-105B	9011
Carrier Amplifier	1-113B	22364
		25136
		17235
		25137
		224DH16
		226DH16
		562DH16
Galvanometers (5)	7-323	N.A.
Galvanometers (3)	7-344	N.A.
Recording Oscillograph	5-124	10190

blade pitch control actuation mechanism in proportion to any combination of a number of command signals. A system electrical schematic is presented in Figure 33 and shows the system consisted of the following:

a. A d.c. power amplifier capable of 40 watts minimum output at ±30 volts

b. A voltage gain stage used for summing and lag equalization

c. A unity gain amplifier used for feedback lead equalization and isolation

d. A unity gain amplifier used for isolation of mode selection and subsumming functions

e. A saturating output integrating amplifier used as a ramp (or step) input generator

f. A 10-slope function generator used to provide an adjustable, nonconstant rate type of input to collective pitch

g. Five 10-turn dial potentiometers and two 10-turn trim pots

h. Various mode-selecting and event switches and a sensitive balance meter

1.3.2 Mechanical System

The blade pitch actuation mechanism was driven by two 1/50-horsepower, permanent-magnet d.c. motors with no-load speeds of approximately 15,000 rpm. These two motors were wired and geared in parallel to drive the 10-turn followup potentiometer and a dual-nut preloaded recirculating ball screw, which in turn drove an actuation shaft concentric to the rotor shaft. A duplex-bearing swashplate was affixed to this shaft to actuate the blade-feathering horns through rod-end links.

1.3.3 System Characteristics

The system was designed to control the rotor in either of two modes of operations, rate (windmilling rpm) or position (feathered-rotor azimuthal position). In the rate mode, the

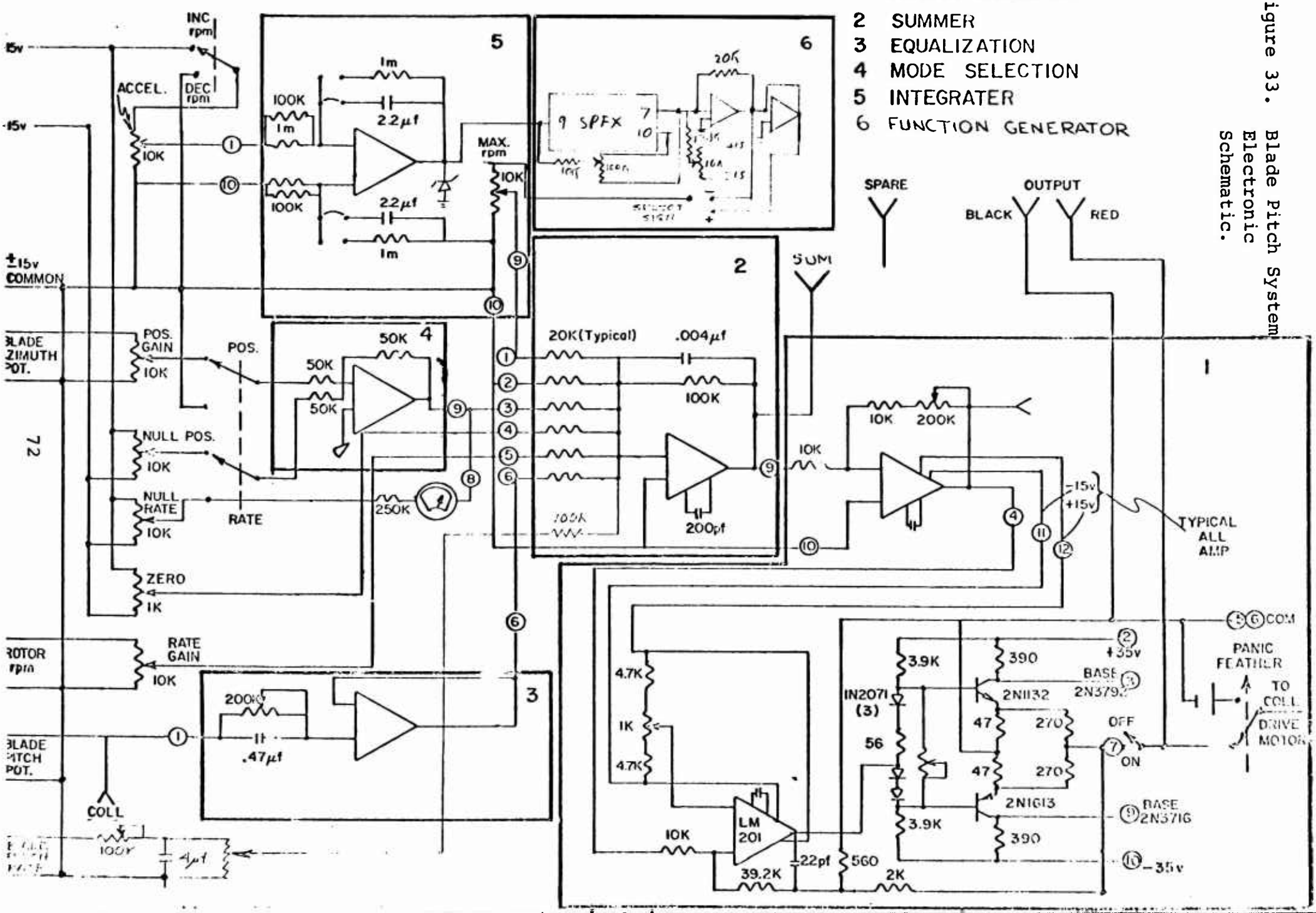

Figure 33. Blade Pitch System Electronic Schematic.

rotor angular velocity was sensed and summed to command blade pitch angle. In the position mode, both angular velocity and rotor azimuth were sensed and summed to command the blade pitch angle.

The basic blade pitch angle control system had a saturating integrator ramp input generator whose rate and amplitude could be adjusted independently. For this test, however, an adjustable, nonconstant rate type of input to collective pitch was required. To accomplish this, a 10-slope function generator was incorporated into the input circuitry.

The function generator (Philbrick-Nexus SPFX-P) used was a biased-diode-type device which, when driven by the voltage ramp from the saturating integrator, gave a ramp output consisting of 10 potentiometer-adjustable slopes between 11 evenly spaced breakpoints. The output of this device in turn was used as the command signal for the blade collective pitch positioning system. In use, a desired collective schedule was synthesized by assuming approximate potentiometer settings for the various slopes between breakpoints and then iterating to the final desired schedule.

To control the blade collective closely in following the commanded programs, it was necessary to increase greatly both the bandwidth and damping of the positioning servo inner loop. This was accomplished by incorporating into the blade positioning system a d.c. tachometer whose output was used as a damping signal for the blade pitch servo.

2. WIND TUNNEL TEST FACILITY

The wind tunnel used for these experiments is located on the Forrestal Campus of Princeton University and is part of the educational and research facilities of the Department of Aerospace and Mechanical Sciences. The tunnel itself is conventional in most respects. Pertinent characteristics are as follows:

a. Test section size - 4 feet high x 5 feet wide

b. Working medium - unconditioned air

c. Maximum steady velocity - 185 ft/sec

d. Minimum steady velocity - 30 ft/sec

e. Closed circuit - oriented in a vertical plane with the return below the test section

f. Closed test section, unvented and nonporous

g. Settling chamber at atmospheric pressure

h. Eddy-current clutch controlled

i. Six-component virtual-center balance with dial readouts

Both tunnel and balance system have been in continuous use since 1950 and have proven to be reliable and accurate.

The dynamic pressure in the wind tunnel test section was measured by means of a pitot-static probe mounted near the tunnel wall just upstream of the rotor plane. A variable-reluctance differential-pressure transducer was used to provide analog voltages for recording purposes.